Thesis for the Degree of Licentiate of Engineering

Transmitter Linearization for mm-Wave Communications Systems

Halil Volkan Hünerli

CHALMERS

Microwave Electronics Laboratory
Department of Microtechnology and Nanoscience – MC2
Chalmers University of Technology
Göteborg, Sweden 2021

Transmitter Linearization for mm-Wave Communications Systems

Halil Volkan Hünerli

Chalmers University of Technology
Department of Microtechnology and Nanoscience – MC2
Microwave Electronics Laboratory
SE-412 96 Göteborg, Sweden
+ 46 (0) 31-772 1000

ISSN 1652-0769
Technical report MC2-440

Printed by Chalmers Reproservice
Göteborg, Sweden 2021

Abstract

There is an ever increasing need for enabling higher data rates in modern communication systems, which brings new challenges in terms of the power consumption and nonlinearity of hardware components. These problems become prominent in power amplifiers (PAs) and can significantly degrade the performance of transmitters, and hence the overall communication system. Hence, it is of central importance to design efficient PAs with a linear operation region. This thesis proposes a methodology and a comprehensive framework to address this challenge. This is accomplished by application of predistortion to a mm-wave PA and an E-band IQ transmitter while investigating the trade-offs between linearity, efficiency and predistorter complexity using the proposed framework.

In the first line of work, we have focused on a mm-wave PA. A PA has high efficiency at high input power at the expense of linearity, whereas it operates linearly for lower input power levels while sacrificing efficiency. To attain both linearity and efficiency, predistortion is often used to compensate for the PA nonlinearity. Yet, the trade-offs related to predistortion complexities are not fully understood. To address this challenge, we have used our proposed framework for evaluation of predistorters using modulated test signals and implemented it using digital predistortion and a mm-wave PA. This set-up enabled us to investigate the trade-offs between linearity, efficiency and predistorter complexity in a systematic manner. We have shown that to achieve similar linearity levels for different PA classes, predistorters with different complexities are needed and provided guidelines on the achievable limits in term linearity for a given predistorter complexity for different PA classes of operation.

In the second line of work, we have focused on linearization of an E-band transmitter using a baseband analog predistorter (APD) and under constraints given by a spectrum emission standard. In order to use the above proposed framework with these components, characterizations of the E-band transmitter and the APD are performed. In contrast to typical approaches in the literature, here joint mitigation of the PA and I/Q modulator impairments is used to model the transmitter. Using the developed models, optimal model parameters in terms of output power at the spectrum mask limit are determined. Using these as a starting point, we have iteratively optimized operating point of the APD and linearized the E-band transmitter. The experiments demonstrated that the analog predistorter can successfully increase the output power by 35% (1.3 dB) while satisfying the spectrum emission mask.

Keywords: linearization, analog predistorter, mm-wave power amplifier, E-band, transmitter, digital predistortion.

List of Publications

Appended Publications

This thesis is based on work contained in the following papers:

[A] H. V. Hünerli, M. Gavell, P. Taghikhani, and C. Fager, "A Methodology for Analysis of mm-Wave Transmitter Linearization Trade-offs Under Spectrum Constraints," Proc. International Workshop on Integrated Nonlinear Microwave and Millimetre-wave Circuits, 2018.

[B] H. V. Hünerli, M. Özen, M. Gavell, and C. Fager, "E-band Transmitter Linearization Using Analog Predistortion," Manuscript.

Acknowledgments

Firstly, I would like to express my gratitude to my main supervisor Prof. Christian Fager and co-supervisor Dr. Marcus Gavell for their guidance throughout this work. I am grateful for the support and the opportunities they have provided during my studies. Without their patience, this work would not have been possible. I would also like to thank Prof. Herbert Zirath for accepting to be the examiner for my thesis.

My sincere thanks to Prof. Thomas Eriksson for our fruitful and efficient discussions. I wish to acknowledge the help provided by Prof. Iltcho Angelov, Dr. Mustafa Özen and Dr. Mattias Ferndahl. The ideas and technical expertise you provided have been very valuable.

I am particularly grateful for the assistance given by Göran Granstrom and Prof. Koen Buisman for making things work in the lab when I were stuck. I would especially like to thank Göran for spending endless hours troubleshooting problems with me during the measurements.

I am indebted to Dr. William Hallberg and Dr. Sebastian Gustafsson for teaching me how to use "stuff" in the lab. Very special thanks to Sebastian for forcefully introducing me to cryptocurrency world, which will hopefully end up better than I now predict.

I would like to thank all of my colleges at Chalmers and Gotmic for providing a good working environment.

Last but not least my beloved wife Ayça. You are always there for me whenever I need it. Thank you for your infinite love, support and patience. Without you this thesis would never have been completed.

This project is financially supported by the Swedish Foundation for Strategic Research. Part of this work has been carried out in the GigaHertz Centre in a joint project financed by the Swedish Government Agency for Innovation Systems (VINNOVA), Chalmers University of Technology, Ericsson AB, Gotmic AB, Infineon Technologies Austria AG, National Instruments, Qamcom, RISE AB, and SAAB AB.

"So long, and thanks for all the fish..."

Douglas Adams

Abbreviations

5G	Fifth Generation Mobile Networks
ADC	Analog-to-Digital Converter
APD	Analog Predistorter
AMAM	Amplitude-to-amplitude
AMPM	Amplitude-to-phase
AWG	Arbitrary Waveform Generator
BER	Bit Error Rate
CW	Continuous Wave
DAC	Digital-to-Analog Converter
DPD	Digital Predistorter
DUT	Device Under Test
EVB	Evaluation Board
EVM	Error Vector Magnitude
GSM	Global System for Mobile
ILA	Indirect Learning Architecture
IoT	Internet of Things
LO	Local Oscillator
LUT	Look-up Table
NMSE	Normalized Mean Square Error
PA	Power Amplifier
PAE	Power Added Efficiency
PSD	Power Spectral Density
QAM	Quadrature Amplitude Modulation
RF	Radio Frequency
RMS	Root Mean Square
RX	Receiver
SNR	Signal to Noise Ratio
TX	Transmitter
VNA	Vector Network Analyzer

Contents

Chapter 1

Introduction

We have seen a rapid development of communication systems since the first deployment of 2G Global System for Mobile (GSM) in the early 90s [1]. As our needs in regard to communication systems changed, the focus of the standards also changed. For instance, 2G was intended for relatively simplistic case of voice communication for improved coverage, whereas 4G potential applications include much more demanding scenarios such as high definition mobile TV and video conferencing [2–4]. The recent and coming 5G standard is expected to go even beyond these scopes with inclusion of millions of Internet of Things (IoT) devices, increased data rates over 1 Gbits and decreased latency at the order of 1-10 ms [5]. According to [6], it is predicted that 5G will occupy half the total mobile traffic by 2025, which is 40% more than today's (summer 2020) global mobile volume.

Modern communication systems require continuously increasing data rates with each generation, for instance from 384 kb/s for 2G, 3 Mb/s for 3G, 100 Mb/s for 4G and up to more than 1 Gbit/s for 5G. There is a similar trend in data transfer rates for other wired and non-wired networks, such as fixed lines and satellite communications. Especially in 2020, with the restrictions and regulations due to the Covid-19, there is an significant increase in demand for the use of communication networks, for instance, due to work from home concept and online meetings. Hence, it is required that the existing resources are used more efficiently and new resources, such as wider bandwidths and new frequency bands, are utilized. Consistent with this necessity, with the upcoming communications generations, soon we will employ mm-waves of the frequency spectrum for daily internet use.

1.1 Background

The front-end of a wireless communication system is comprised of a transmitter (TX) and a receiver (RX). A simple block diagram of such a communication system can be seen in Figure 1.1. At the TX end, digital data comprised of bits is converted into an analog signal via a digital to analog converter (DAC). This signal is then upconverted to a carrier frequency using a mixer, boosted with a power amplifier (PA) and then sent over air using an antenna. The RX follows this process in reverse order until the analog signal is converted back to

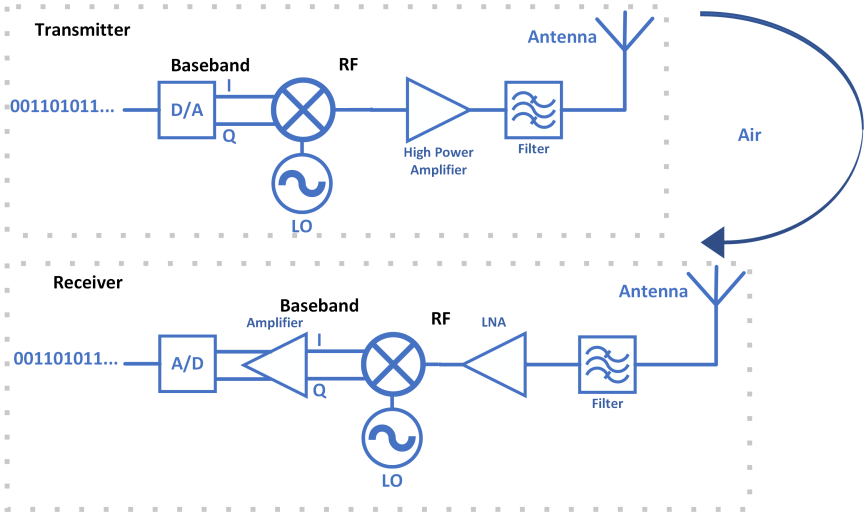

Figure 1.1: Transmitter block diagram.

digital.

Two commonly used approaches for increasing the data rate of a communication system are using increased modulation orders and larger bandwidths. The first method requires the use of more bits per a data symbol. Since increasing the modulation order results in higher bit error rates (BER) for the same average power levels, higher signal to noise ratio (SNR) is needed to achieve the same BER using increased modulation orders. This results in higher output power requirements. However, the power cannot be increased without a limit due to emission regulations rising from health concerns and due to limitations with the hardware. To increase the data rate, one may increase the modulation order, but this requires higher SNR, hence, increasing the power. At some point, the power level breaches the power limits [7] and it becomes more practical to increase the bandwidth instead of increasing the modulation order. With the crowded state of the current communication bands, carrying signals to higher frequencies has become an attractive solution to increase the bandwidth. For example, the 60 GHz band defined for IEEE 802.11ad covers the band from 57 to 71 GHz [8]. Recently, SpaceX applied for 71-86 GHz Band (E1 and E2 bands) for use of high bandwidth communications using satellites [9].

The aforementioned higher frequency bands bring significant challenges in terms of both hardware design and signal processing [10–12]. At higher frequencies, the gain, hence the efficiency is decreased due to the limitations in f_T and f_{MAX} of the used transistors. Here, f_T and f_{MAX} are the cut-off frequency and the maximum frequency of oscillation respectively. One of the most influential components for the overall efficiency of a communication system is the power amplifier at the transmitter. Using the transmitter at its high efficiency region becomes more important, although behavior of a typical transmitter is highly nonlinear in this region. This nonlinear behavior causes both in-band signal distortion and spectral regrowth. While in-band distortion causes difficulty for signal recovery, spectral regrowth causes interference in neighbouring channels. To prevent these effects, the PA can be operated at

a linear backed-off state, where the efficiency is very low. Hence, there is an underlying trade-off between linearity and efficiency.

This trade-off can be improved by a combination of two approaches; using high-efficiency power amplifiers which have improved efficiency even at backed-off powers, and using in- and out-band distortion compensation of distortion that the amplifiers introduce. Generally, digital predistortion techniques (DPD) are implemented to linearize the transmitted signal due to ease of implementation. On the other hand, analog predistotion (APD) has the potential of increasing the power efficiency of the system while reducing the computational requirements, which is not straightforward to achieve with digital predistortion.

1.2 Motivation

The TX should both be energy efficient and linear. Especially in mm-wave, a conventional TX uses a class A/AB power amplifier to satisfy high gain requirements (in a small device area), which is usually linear but not energy efficient. For a TX, the nonlinearities include harmonic distortion, gain compression, phase distortion, phase noise, intermodulation distortion, etc. This thesis focuses on gain compression, phase distortion and intermodulation distortion, which are typically the more dominant ones.

For an active device such as a PA, when the frequency is increased, the gain drops due to the intrinsic capacitances of the transistors. This also causes the efficiency to drop significantly. As mentioned above, the transmitters are used at their back-off regions to remedy the nonlinear effects. In this region the efficiency drops even further. As a comparison, at 1.95 GHz it is possible to see an efficiency of more than 50% at 6 dB back-off [13] while at E-band this value can easily drop below 5%. Consequently, it becomes critical to address this issue. One important method is using linearization techniques. It is possible to categorize these techniques according to their working principle, operating frequency or whether it is in analog or digital domain. With digital predistortion, it is possible to employ very accurate and higher order functions to compensate for the nonlinearities. Analog predistorters potentially have lower energy consumption and can provide larger bandwidth of operation compared to their digital counterparts. Hence, linearizer choice is of utmost importance for mm-wave systems due to power, linearity and efficiency trade-offs.

1.3 Objectives of the Thesis and Outline

This thesis addresses the above challenges by application of predistortion to a PA and an IQ transmitter while investigating the trade-off between linearity, efficiency and predistorter complexity, using a systematic and comprehensive framework. The objectives can be listed as follows:

- Create a framework for evaluation of predistorters using modulated test signals
- Implement the framework using digital predistortion and a mm-wave PA

- Investigate the trade-offs between linearity, efficiency and predistorter complexity using this framework
- Characterize an E-band transmitter and an analog predistorter in order to use these as central components of this framework
- Linearize the E-band transmitter using the analog predistorter and increase the output power while satisfying a spectrum emission mask

The thesis is organized as follows. In this chapter we presented the motivation for the thesis. Chapter 2 presents behavioral modeling and characterization methods for transmitters. In Chapter 3, linearization techniques and applications are explained. Furthermore, a general framework for evaluation of predistorters is presented. In Chapter 4, predistortion of mm-wave transmitters is presented including an implementation in E-band. Finally, conclusions and future work are provided in Chapter 5.

Chapter 2

Characterization and Modeling of a Transmitter in a Communication System

A behavioral model provides a mathematical representation of the output of a system in terms of its input. This model is typically constructed using recorded input-output pairs for that system [14]. Behavioral models are used to describe the input-output relationship with good accuracy and low computational effort. Behavioral modeling is a powerful tool that can serve as an intermediate step for design of compensation schemes for nonlinearities introduced by a device, in our case the amplitude and phase distortions introduced by a power amplifier or a transmitter. In particular, distortion compensation, or linearization, can be best cast as a multi-step procedure. First, we characterize the device using a large dataset of input-output observations. Then, the model is used to find the inputs that will create the desired outputs. A detailed and an accurate model is crucial since this model is used to identify the predistorter that effectively 'inverts' the nonlinear behavior of the device.

This chapter presents a short review of characterization and behavioral modeling of power amplifiers and transmitters. In Section 2.1, different characterization methods for these devices are presented. Section 2.2 gives an introduction to behavioral modeling for PAs and TXs. Finally, in Section 2.3, characterization and modeling of a direct conversion transmitter is presented.

2.1 Characterization Methods

Device characterization provides the data needed for model extraction. The characterization process and its accuracy influences the resulting model. In particular, for behavioral modeling of a PA or TX, the measurements consist of a set of input data and a corresponding set of output data acquired through a measurement device like an oscilloscope or a vector network analyzer (VNA).

The measurement, hence the characterization result, depends on the excitation signal type. In this section, some of the regularly used characterization methods for these devices are summarized.

2.1.1 Energy Efficiency

While not a part of behavioral modeling, an important step in characterization of a device is device efficiency calculations. When an input signal is fed to the device under test (DUT), the instantaneous DC power consumption is also recorded along with the output of the device, which then can be used for efficiency calculations. These numbers should be recorded for different amplitude levels of the input signal to get accurate efficiency values. Two commonly used ways to calculate the efficiency are drain efficiency and power added efficiency (PAE). Drain efficiency (η) is the ratio of the output RF power to the DC power consumption, whereas PAE is calculated by subtracting the input RF power from the output in the numerator of η;

$$\begin{aligned} \eta &= P_{RFout}/P_{DC} \\ \text{PAE} &= (P_{RFout} - P_{RFin})/P_{DC}. \end{aligned} \tag{2.1}$$

2.1.2 Single-tone Characterization

For a single-tone, or continuous wave (CW) signal, amplitude-to-amplitude (AMAM) and amplitude-to-phase (AMPM) conversion measurements are used for parametrizing typically nonlinear static memoryless models or models with linear memory. For obtaining AMAM and AMPM data, often a large signal VNA is employed whereas, a large signal network analyzer or an oscilloscope constitute viable alternatives.

The VNA performs measurements by using the incident and reflected waves at the input and the output of a DUT. CW measurements are performed at a single frequency using the source of the VNA. To generate a detailed response, hence a more accurate model, excited signal should push the DUT to its saturation. Using this method, complex gain and efficiency of the device is measured versus the input power, if DC consumption is also acquired. For each amplitude of the CW input, we obtain a corresponding output amplitude and phase, which in term gives us AMAM and AMPM. An example to this characterization method using a mm-wave PA is given in Chapter 4.

2.1.3 Two-tone Characterization

Two-tone characterization is another important approach to obtain nonlinear amplifier characteristics. The excitation signal is created by sum of two signals at different but closely separated frequencies [15]. Intercept points such as IP3 can be extracted from these measurements. Furthermore, when different power levels and frequency spacings are used, we can get some insight about the memory effects that exist in the amplifier [16].

The excited input signal is created using two signal generators and output is usually monitored with a spectrum analyzer, vector signal analyzer, or an oscilloscope. The oscilloscope or vector signal analyzer data can be used for model creation. The spectrum analyzer lacks the phase information, hence the

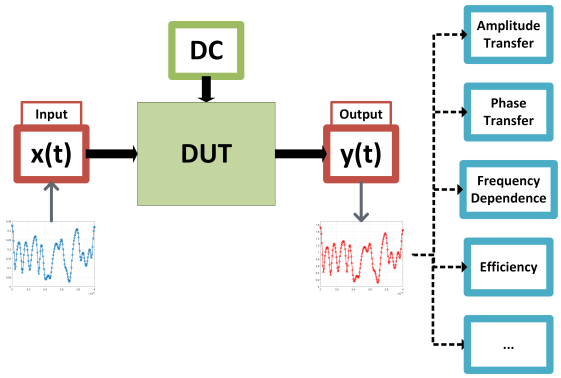

Figure 2.1: Schematic diagram of the characterization of a device under test (DUT) using a modulated signal. x(t) and y(t) represent the time domain representations of modulated input and output signals, respectively.

corresponding model would be limited. When the DUT is operating around its nonlinear region, intermodulation distortion creates components at other frequencies at sum, difference and harmonics of the input signals. This effects cannot be observed when a single-tone input signal is used.

2.1.4 Characterization Using Modulated Signals

Another method of characterization is using modulated signals with a specific bandwidth. This allows us to test a device with real communication signals. Hence, using modulated signals is a practical and realistic way to characterize the device, while at the same time getting insight about in-and out-band frequency response. With this method, it is possible to extract nonlinear memoryless models as well as models with linear and nonlinear memory. Furthermore, we achieve flexibility in characterization with the ability to change the test signal's modulation order and bandwidth in addition to its amplitude. Hence, we obtain a more accurate model that also gives the wide-band characteristics of the device.

Figure 2.1 presents a block diagram for the characterization of a DUT using modulated signals. A modulated signal (x(t)) is fed to the DUT. The output signal (y(t)) is also recorded, together with the instantaneous DC power consumption. From this recorded information, all the blocks given at the output in Figure 2.1, amplitude transfer, phase transfer, frequency dependence, efficiency, etc., can be retrieved.

In particular, in frequency domain, the input signal covers a certain bandwidth around a center frequency f_0. If the device is a transmitter, f_0 can be changed by sweeping the frequency of the local oscillator (LO), see Figure 2.1. By comparing the input and the output signals, the amplitude and phase transfer characteristics can be found. This response changes for different f_0 values. Moreover, using the recorded power consumption, it is possible to calculate efficiency of the device. It is important to note that, memory effects are present for a wide band signal at a fixed center frequency. In addition to the aforementioned effect, for a signal, different frequency regions may exhibit different response profiles, which translates to memory in behavioral models.

2.2 Behavioral Modeling

In a transmitter, the main source of nonlinearity is power amplifiers in combination with frequency mixers. For a single RF component, such as a PA, it is comparatively easy to characterize the input-output relationship. For a system with many such components, like a TX, this relation becomes more complicated. Multiple component models should be connected to each other to create the overall input-output relation. Then, it becomes attractive to address the modeling problem by treating the system as a whole instead of using the models of the individual components.

Modern predistortion techniques rely on identifying the nonlinear dynamic response of the TX. To increase the power efficiency of the system, the PAs should be operated as close as possible to saturation, where the nonlinearities are strong. Then, the resulting model of the system is expected to include these nonlinearities. During modeling, it is beneficial to categorize the type of nonlinearity system exhibits into two main groups: static and dynamic nonlinearity.

Static nonlinearity is related to the nonlinear DC characteristics of the transistors. In this kind of nonlinearity, the instantaneous output signal is only related to the instantaneous input signal [17]. This is the major nonlinearity source in the device.

Dynamic nonlinearity can arise from the interaction between the transistor nonlinearities and linear dynamic effects such as matching networks' frequency response. These dynamical effects are called memory effects. Here, the instantaneous output signal is influenced by the previous instants of the signal in addition to the present signal [14]. The dynamic changes in the system due to frequency response are called short-term memory effects due to small time constants when compared to the changes in the envelope of the RF signal. Long-term memory effects have large time constants compared to the RF signals and can arise from non-ideal bias networks and temperature changes due to power dissipation [17].

A power amplifier's representative nonlinear function maps an RF input signal to an RF output signal [18]. On the other hand, a direct conversion TX usually has an upconverting mixer, meaning that the baseband input signal is mapped to the RF output signal. However, the information carried by a narrow band RF signal, $u_{RF}(t)$, around a center frequency f_c can be represented by its complex baseband equivalent, $u(t)$ [19]. The relation between them is as follows

$$\begin{aligned} u_{RF}(t) &= A(t)cos(\omega_c t + \phi(t)) \\ &= Re\{u(t)e^{j\omega_c t}\}, \end{aligned} \tag{2.2}$$

where $u(t) = A(t)e^{j\phi(t)}$. Here, $A(t)$ and $u(t)$ are amplitude and phase modulations, respectively, and $\omega_c = 2\pi f_c$ is the carrier frequency. Equation (2.2) represents the conversion between the carrier frequency and baseband. Using this relation, the models can be created. With the use of higher frequencies, the computational complexity of performing the necessary operations at the RF band increases. In particular, it becomes more practical to use baseband approach due to its lower sampling rate requirements during signal acquisition.

As a result, the models considered in this chapter are in complex baseband domain.

Traditionally, behavioral models are classified according to what kind of memory effects they can describe [17, 20, 21]. Behavioral models for single input-single output PAs can be divided into three categories: memoryless models, models with linear memory and models with nonlinear memory. In the upcoming sections, we explain these models in more detail.

2.2.1 Memoryless Models

Memoryless models are based on quasi-static AMAM and AMPM conversion properties of the device. Here, they represent the amplitude and phase distortion at the output as a function of the input signal amplitude. They provide acceptable accuracy when there is very limited or no memory effects in the device. Several memoryless models have been proposed in literature, such as Saleh models, polynomial models and simple look-up tables (LUT) [17, 22]. The most commonly used ones are polynomial or power series model and the LUT model.

The most basic technique to characterize the behavior of PAs is by using LUT models. Here AMAM and AMPM of the device is acquired by measurements and stored in LUTs. For a specific input amplitude, a corresponding output amplitude and phase conversion is mapped.

Another commonly used memoryless model is the polynomial model. For this model, the input-output relationship is given as

$$y_{RF}(t) = \sum_{p=0}^{P} a_p x_{RF}^p(t) \tag{2.3}$$

Here, $x_{RF}(t)$ and $y_{RF}(t)$ are the input and output signals of the device, respectively. The coefficients of the polynomial are denoted with a_p. We can derive an approximate output signal by starting from (2.3) and substituting (2.2). For this specific example, we assume that $P = 3$ for simplicity and we get

$$\begin{aligned} y_{RF}(t) &= a_0 + a_1 A(t) cos(\omega_c t + \phi(t)) + a_2 A^2(t) cos^2(\omega_c t + \phi(t)) \\ &\quad + a_3 A^3(t) cos^3(\omega_c t + \phi(t)) \\ &= a_0 + [a_1 A(t) + \frac{3a_3 A^3(t)}{4}] cos(\omega_c t + \phi(t)) \\ &\quad + \frac{a_2 A^2(t)}{2} cos(2\omega_c t + 2\phi(t)) + \frac{a_3 A^3(t)}{4} cos(3\omega_c t + 3\phi(t)), \end{aligned} \tag{2.4}$$

At the output, we see that signals at DC, $2\omega_c$ and $3\omega_c$ are also created. When the bandwidth of the signal is sufficiently small compared to the carrier frequency, higher harmonics will be far away from the carrier frequency when compared to the signal bandwidth. In such cases, higher harmonics can be filtered out. DC component is blocked by a capacitor along the RF line. Then, the remaining component in carrier frequency can be represented in baseband as

$$\begin{aligned} y(t) &= a_1 A(t) e^{j\phi(t)} + \frac{3a_3}{4} A^3(t) e^{j\phi(t)} \\ &= a_1 x(t) + \frac{3a_3}{4} x(t)|x(t)|^2 \end{aligned} \tag{2.5}$$

Here $x(t)$ and $y(t)$ are the baseband equivalents of $x_{RF}(t)$ and $y_{RF}(t)$. Using (2.5), we can create a baseband model of arbitrary order as follows:

$$y(n) = \sum_{p=0}^{P} a_p x(n)|x(n)|^{2p} \tag{2.6}$$

In (2.6), it can be observed that only odd-order terms are present. The reason for this is due to the distortion contribution introduced by the even-order terms being far away from the carrier frequency [23]. Although many publications focus only on odd-order terms, it has been shown that more accurate models can be obtained if even-order terms are also included [24].

Using memoryless models can significantly simplify behavioral modeling. Static models, such as AMAM and AMPM representations are frequency independent and are accurate for narrow band signals. When the signal bandwidth increases, memory effects become more apparent and the memoryless models no longer have acceptable performance.

2.2.2 Models with Memory

The drawback of memoryless models is that they are limited to a narrow band signals and the changes due to frequency, hence memory effects, are not represented. This frequency dependent behavior may include AMAM, AMPM or a combination of two at different frequency regions of the device. The models created may handle nonlinearity using either linear or nonlinear memory.

Nonlinear models with linear memory introduces linear filters to the system. The memory effect is modeled by the cascade combination of linear filters and the memoryless nonlinearity. The simplest cases are the Wiener model and the Hammerstein model [17]. For the Hammerstein model, nonlinearity is followed by a linear filter and for the Wiener model, a linear filter is followed by nonlinearity, which are so called two-box models. It is possible to get a more accurate linear memory by implementing a combination of the two using filter-nonlinearity-filter model structure.

When a broadband signal is used, some dynamic effects show up in nonlinear regimes that cannot be modeled with linear memory. This is due to dynamic interaction of more than one nonlinearity interacting with each other, where a non-interacting linear filter is not enough for accurate model creation [14]. With the use of wider band signals, models with nonlinear memory becomes a necessity. In the literature, there exists several modeling approaches including time-delay neural network model, nonlinear autoregressive moving-average model and polynomial based models [20]. In this thesis, polynomial based models are used due to their ease of identification.

The most basic and widely used modeling method using nonlinear memory is the memory polynomial model and it is quite accurate for weakly nonlinear systems [17, 22, 23, 25, 26]. For such a system, the memory polynomial model can be expressed as

$$y(n) = \sum_{m=0}^{M} \sum_{p=0}^{P} a_{p,m} x_{n-m} |x_{n-m}|^{2p}, \tag{2.7}$$

where $a_{p,m}$ are the model coefficients. Here, M and P represent the memory depth and the maximum polynomial order of the model, respectively. For direct conversion transmitters, in contrast to PAs, the in- and quadrature phase baseband components are fed to separate inputs. An expansion to the model presented here is considered in the next section that accepts multiple inputs to the model.

2.2.3 Memory Polynomial Model for I/Q Modulation Impairments

The IQ modulator at direct conversion transmitter transforms the complex baseband signals to passband signals centered at the carrier frequency. An ideal IQ modulator provides two orthogonal channels for the real and imaginary parts of the complex baseband signal. In practice, IQ modulator introduces some degree of interference between these two orthogonal channels, resulting in IQ imbalance. In order to model this IQ imbalance, the model described in Section 2.2.2 need to be modified so that additional non-linear effects, such as IQ imbalance, can be represented properly.

Compensation of IQ imbalance for a wideband channel is investigated in [27] and [28]. Generally, for a device with separate I/Q inputs one can describe the output as a nonlinear function of the input x and its conjugate, x^* [29]. The modeling of the IQ imbalance is thus achieved by adding a function of x^* to the memory polynomial. This approach is based on [28], where the DPD design for joint mitigation of a power amplifier and I/Q modulation impairments is investigated. Therefore, nonlinear functions of the following form is considered

$$f_1(x_n, \ldots, x_{n-M}) = \sum_{m=0}^{M} \sum_{p=0}^{P} (a_{2p,m}) x_{n-m} |x_{n-m}|^{2p} \tag{2.8}$$

$$f_2(x_n^*, \ldots, x_{n-M}^*) = \sum_{m=0}^{M} \sum_{p=0}^{P} (b_{2p,m}) x_{n-m}^* |x_{n-m}^*|^{2p} \tag{2.9}$$

where $x_n = I_n + jQ_n$. Here, $a_{2p,m}$, $b_{2p,m}$ are unknown complex coefficients associated with $f_1(\cdot)$ and $f_2(\cdot)$, respectively. The number of memory taps is given by M and the nonlinear polynomial order of the system is given by P.

Let us define

$$f_{1,n} \triangleq f_1(x_n, \ldots, x_{n-M}) \tag{2.10}$$

$$f_{2,n} \triangleq f_2(x_n^*, \ldots, x_{n-M}^*) \tag{2.11}$$

The output at time n, i.e. y_n, is given by $y_n = f_{1,n} + f_{2,n}$. For a set of measurement data, this input-output relationship can be expressed as follows

$$\mathbf{y_{mod}} = \mathbf{H}\boldsymbol{\theta}, \tag{2.12}$$

where $\boldsymbol{\theta}$ are the complex coefficients $a_{2p,m}$ and $b_{2p,m}$ in vector form as follows

$$\begin{aligned}\boldsymbol{\theta} =&[a_{0,0}, \ldots, a_{2P,M}, \\ &b_{0,0}, \ldots, b_{2P,M}]^T.\end{aligned} \tag{2.13}$$

The modeling realized in Chapter 4 uses the memory polynomial model, which can be considered as an extended version of the polynomial model with linear memory, which also includes nonlinear memory through high order terms.

2.2.4 Model Coefficient Estimation

In (2.12), $\mathbf{y_{mod}}$ is the model outputs y_n in vector form and $\mathbf{H} = \mathbf{H}(\mathbf{x}, \mathbf{x}^*)$ is the nonlinear memory polynomial elements $x_{n-m}|x_{n-m}|^{2p}$ and its conjugate in $f_{1,n}$ and $f_{2,n}$ in matrix form, respectively. $\mathbf{H}$ can be created as follows

$$\mathbf{H}(\mathbf{x}, \mathbf{x}^*) = \begin{bmatrix} x_n & x_n^* & \ldots & x_n|x_n|^{2p} & x_n^*|x_n|^{2p} \\ \vdots & \vdots & \vdots & \vdots & \vdots \\ x_{n-m} & x_{n-m}^* & \ldots & x_{n-m}|x_{n-m}|^{2p} & x_{n-m}^*|x_{n-m}|^{2p} \end{bmatrix} \tag{2.14}$$

Let $\mathbf{y}$ denote the data that is collected with a measurement setup. Then, the unknown coefficients $\boldsymbol{\theta}$ can be estimated by finding the least-squares solution. In particular, the estimate of $\boldsymbol{\theta}$ is given by

$$\hat{\boldsymbol{\theta}} = (\mathbf{H^H H})^{-1}\mathbf{H^H y} = \mathbf{H}^+\mathbf{y}, \tag{2.15}$$

where $\mathbf{H}^+$ is the Moore-Penrose inverse and $\mathbf{H^H}$ is the Hermitian of $\mathbf{H}$. Each estimated coefficient is then used to create the transfer function of the system block of interest, the TX for our case.

2.3 Characterization and Modeling of a Direct Conversion TX

Different characterization and modeling methods summarized above can better be understood when it is exemplified with a direct conversion TX. In this section, we provide such an illustration.

2.3.1 Characterization of the TX

For a PA, the input-output relationship can be defined by its AMAM and AMPM characteristics. For a direct conversion TX, this definition becomes more complicated. While a PA amplifies an RF signal, an direct conversion TX upconverts a baseband signal with separated I and Q channels to a single RF output.

We now provide a short illustration of characterization of a direct conversion TX. More details and further discussions will be presented in Chapter 4. The block diagram of the measurement setup used for the characterization of such a device can be seen in Fig. 2.2. This is the setup we have used in [Paper B]. Here, a signal is fed to the I and Q channels of the TX from the dual-channel AWG, which is then upconverted to RF by the TX. Before downconversion back to

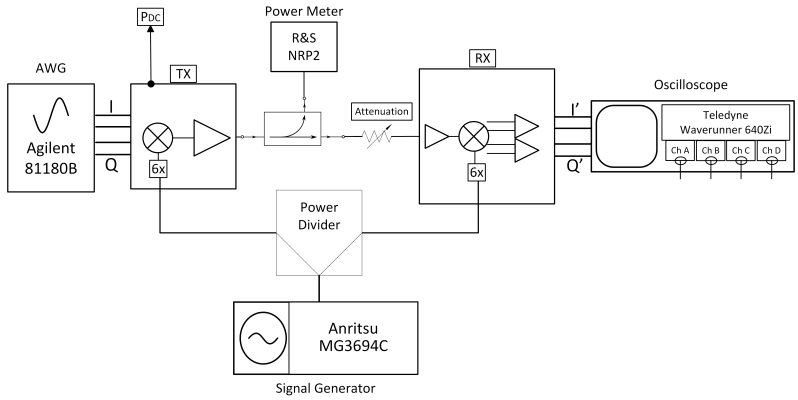

Figure 2.2: Measurement setup for TX characterization. A set of DC or a modulated signal is sent from the arbitrary waveform generator (AWG) to the separate I and Q channels and upconverted via the transmitter. The root mean square (RMS) output power of the RF signal is monitored with a power meter. Thereafter, the RF signal is downconverted with a quadrature receiver and the time domain signal is recovered from the oscilloscope.

baseband with the RX, the signal is attenuated to achieve a compromise between the RX contribution to amplitude/phase compression and RX contribution to the SNR. In particular, the former is minimized as much as possible while keeping the SNR at a high level. We set the attenuation such that the dominant nonlinear contribution came from the TX and no additional spectrum growth due to the RX was received. A directional coupler is used after the TX to measure the output power using a power meter and calibrate the absolute power level of the signal measured with the oscilloscope. This method allows us to predict dynamic I/Q input-to-RF output response and create a model of the TX.

The experiments are performed with different types of signals, e.g. single tone or modulated, at different power levels and bandwidths. Single tone characterization allowed us to create a basic model at a certain frequency. The modulated signal covers a certain bandwidth, so the model created with this method also includes memory effects. Even though the modulated signal characterization facilitates creation of more accurate models, the associated experimental procedure, including signal acquisition and computation time, is slower compared to that of single tone characterization. Moreover, modulated signals with different bandwidths can be used to get more flexibility for nonlinear dynamic modeling. Such experiments can be implemented with our experimental setup and one illustration is given in Section 2.3.2, where modulated signals with 100, 250 and 500 MHz bandwidths are used for model creation.

Figure 2.3 presents the input vs output response curves of MTX0017, an E-band direct conversion TX by Gotmic. Here, input power is swept for both I and Q channels using DC signals and the output power is recorded. On the left, we see a voltage sweep including positive and negative values versus the output power and on the right, we see input power of I and Q channels versus the output power. The characterization of a TX in this manner allows us to more clearly visualize the possible imbalance between I and Q channels while

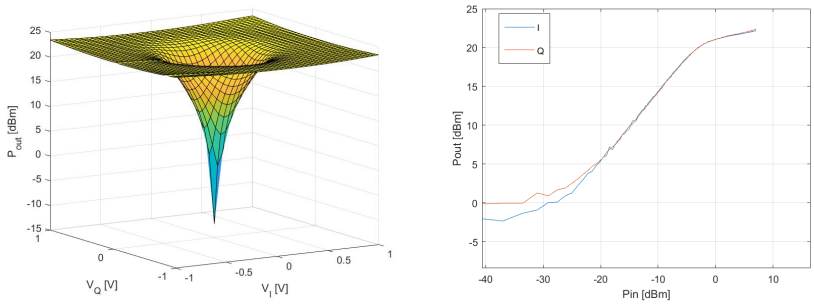

Figure 2.3: Input-output response of a direct conversion transmitter. Output power vs positive and negative I and Q voltage levels (left). Output power vs I and Q power levels (right)

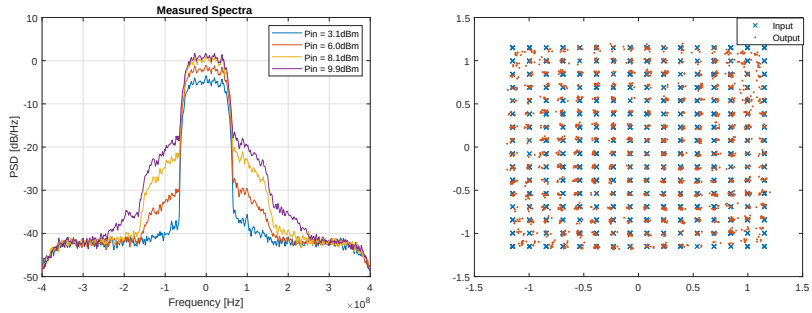

Figure 2.4: The power spectral density (PSD) of the output of the TX for different input power levels (left) and an example constellation diagram (right) at $P_{in} = 8.1$ dBm

applying linearization later on.

Another possible method of characterization is by using a modulated signal. Figure 2.4 presents the power spectral density (PSD) of the output of the TX for different input power levels (left) and an example constellation diagram (right) at $P_{in} = 8.1$ dBm. Here, a randomly generated 256 QAM signal with 100 MS/s, shaped with a raised-cosine-filter using a roll-off factor of 0.3 is tested. The power level of the test signal is gradually increased so that the in- and out-band distortion can be observed. On the left of Figure 2.4, we can see the change in adjacent channels with increasing power. We can also observe from the constellation diagram how the low power parts of the test signal is transferred linearly to the output, while high power parts are distorted. Using this characterization method, it is possible to generate behavioral models of devices as it will be explained further in Section 2.3.2.

2.3.2 Modeling of the TX

For the same TX presented above, a nonlinear memory polynomial can be created following the expressions in (2.8)-(2.9) given in Section 2.2.3. Here, a wideband 256-QAM modulated signal with 192 MS/s is used for excitation. It is important to choose M and P values carefully in (2.8) and (2.9) in order to reach an accurate representation of the measurements. For this specific example

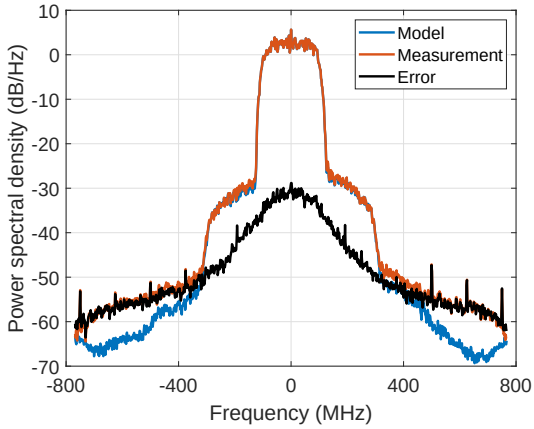

Figure 2.5: Comparison of the measured spectrum of a modulated signal with the model and the error spectrum for a 256QAM signal with 192MS/s. Model has M=5 and P=7 with a resulting NMSE of -30dB.

Table 2.1: Comparison of the model to the measured data for different bandwidths, memory taps (M) and polynomial orders (P).

		NMSE [dB]		
M	P	100 MS/s	250 MS/s	500 MS/s
1	1	-26.74	-24.38	-23.29
3	1	-29.58	-26.48	-25.73
3	2	-30.11	-29.14	-27.86
5	3	-30.32	-29.54	-28.65

we used a $P = 3$ and $M = 5$, meaning a 7th order polynomial with 5 memory taps. The signal is shaped with a raised cosine filter using a roll-off factor of 0.3. Figure 2.5 presents a spectrum plot of the model, the measurement and the error between the two. For this set of M and P values, we get a normalized mean square error (NMSE) value of -30 dB, which shows a good agreement between the measurements and the model.

A more detailed analysis was performed by using different sets of M and P and for different symbol rates. NMSE values for different polynomial orders and memory taps are shown in Table 2.1 for signals with 100, 250 and 500 MS/s. From the table we can observe the following results:

- For a given complexity, i.e. fixed P and M, the NMSE drops with increasing bandwidth.
- Increasing P and M provides improvement in NMSE with diminishing returns. For instance for a symbol rate of 250 MS/s, we observe significant improvement in NMSE until $P = 2$ and $M = 3$, whereas the next complexity level offers minor improvement in comparison.

In this chapter, we have summarized characterization and behavioral modeling of power amplifiers and transmitters. We have also illustrated characterization and modeling of a direct conversion TX for different model orders and data rates. In the next chapter, an overview of predistortion techniques will be presented. In Chapter 4, these techniques and the models developed in this chapter will be brought together to linearize a mm-wave PA and an E-band TX.

Chapter 3

Predistortion Linearization of Wireless Communication Transmitters

To reduce distortion in power amplifiers and transmitters, a direct solution is backing the power off to a region of operation where nonlinear effects are minimal, even if this means loosing efficiency and output power. This can be problematic, especially in mm-wave systems where power budgets are tight, and backing-off of power may result in budget violations. An attractive solution for reducing the distortion is using linearization techniques, which enable more output power and higher efficiency compared to using the PA or the TX at backed-off powers.

A wide range of linearization techniques have been studied in the literature, including feedback, feedforward and predistortion [14, 17, 30]. Most of the modern communication systems use the latter due to the good trade-off between ease of implementation and performance [14, 17]. With behavioral modeling and characterization techniques explained in Chapter 2, a model that describes the nonlinear behavior of the PA or transmitter is found. A predistortion linearizer applies the inverse of this function to compensate for the nonlinear behavior. The aim is to achieve an output signal such that, it is a linear replica of the input signal.

In this chapter, digital and analog predistortion techniques and their applications are summarized. In Section 3.1, predistortion is clarified in terms of implementation frequency. Section 3.2 and 3.3 explains digital and analog predistortion and their parameter identification methods respectively.

3.1 IF, RF and Baseband Predistortion

Predistortion is a linearization technique for a device that has a nonlinear input-output relationship, for instance a PA or a TX. The predistorter is cascaded to the input of the nonlinear device. It creates a distortion characteristic which is the inverse of the distortion characteristics of that device [30]. The aim is to

have a resulting overall system which has a linear input-output relationship in the intended range of operation and has little to none input-output distortion.

In a frequency converting system, several locations exists where predistortion can be implemented: at baseband, IF or RF. The predistortion methods can be classified according to these locations [30]. We will now discuss these predistortion methods in the upcoming sections.

3.1.1 IF Predistortion

IF predistortion is located at a convenient intermediate frequency. Block diagram of an IF predistorter can be seen in Figure 3.1. In the figure, we can see that the IQ modulated signal is upconverted to the IF frequency. The predistorted signal is then upconverted to the carrier frequency. It has some advantages over its RF counterpart. It can be applied to systems working with different RF frequencies, while utilizing the same IF frequency. Both analog and digital domain implementations are possible, while the latter requires substantial sampling rate for mm-wave applications. A 0.18 µm CMOS 2.4 GHz IF predistorter with controllable gain expansion up to 20 dB is reported in [31] for the linearization of a 42 GHz TX module. Another such implementation is reported in [32] with a 40.5 to 43.5 GHz DPD platform with a fixed IF frequency of 2.1 GHz.

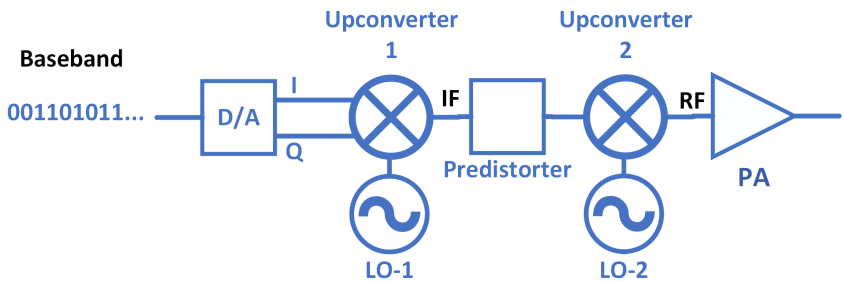

Figure 3.1: Block diagram of a IF predistorter.

3.1.2 RF Predistortion

Here, the predistortion element operates at the final carrier frequency. A basic block diagram of RF predistortion can be seen in Figure 3.2. For mm-wave systems, it becomes challenging to process signals with large bandwidths due to the required high sampling rates [33].

For the analog circuit counterpart, linearization using analog predistortion has been reported up to W-band [34–37]. [37] reports a 5th degree polynomial RF predistorter for linearization of 2.1 GHz PA. A 44 GHz APD using a shunt cold mode HEMT is used to linearize a mm-wave PA in [35]. A traveling wave tube amplifier is linearized using an 81-86 GHz APD design based on an inline active FET nonlinear generator in [36]. The gain expansion characteristics of a Class C amplifier is used for linearization of a GaAs APD and PA chipset at the E-band in [34]. In [38], a cascade combination of DPD and APD is used to address different intermodulation distortions of an RF transmitter.

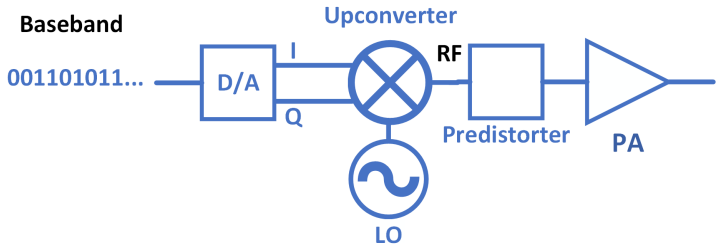

Figure 3.2: Block diagram of a RF predistorter.

3.1.3 Baseband Predistortion

A block diagram of a baseband predistorter can be seen in Figure 3.3. Here the communication signal is upconverted to the carrier frequency after predistortion. Baseband predistortion can be implemented in either analog or digital domains, while the digital implementation (DPD) is the most common. However, the analog baseband PD also has some advantages as will be discussed later. Implementation of complex nonlinear transfer characteristics is easier at baseband when compared to implementations in IF or RF [30]. One frequently used way to implement the AMAM/PM characteristics to predistort the baseband signal before upconversion is using a lookup table [39–41]. A power scalable DPD with a Volterra based model is designed, and applied to a 3.6 GHz TX for linearization in [42]. IQ imbalance corrections are needed for a transmitter with I and Q inputs at the baseband. Compensation for both the nonlinearities and IQ imbalance for a wideband channel is investigated in [28] and [43].

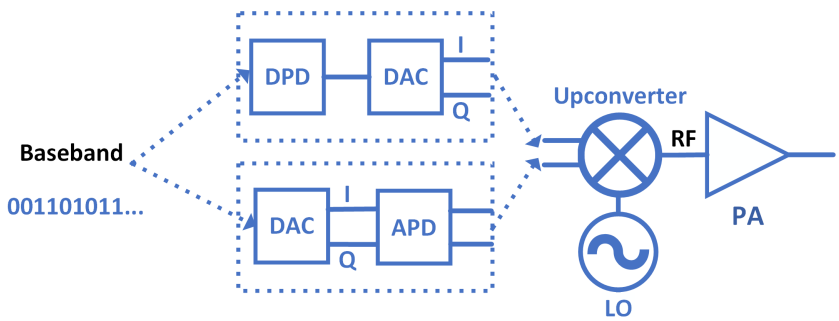

Figure 3.3: Block diagram of a baseband predistorter. Two alternative solutions are given: 1) Digital linearizer, where the DAC is after the DPD (top). 2) Analog linearizer, where the DAC is at the input of the APD (bottom).

3.2 Digital and Analog Predistortion and Parameter Identification

The implementation of predistortion can be in either analog or digital domains. In this section, a general information about digital and analog predistorters are presented including parameter identification.

3.2.1 Digital Predistortion

DPD is the most widely used linearization technique in today's communication systems. DPD uses digital signal processing techniques to predistort a signal before upconversion and amplification by the PA. This combination of the DPD and PA/TX is implemented to achieve a linear input-output response. DPD allows implementing more complex and accurate linearization functions compared to APD, hence facilitating better distortion suppression [44]. However, with DPD, nonlinear baseband signals are generated with larger bandwidths than the signal itself. This results in faster sampling rate, hence larger DAC power consumption for wideband signals.

The distortion correction can take place at baseband, IF or RF as discussed above. DPDs for PAs can be implemented by finding the inverse of the PA, whose input-output relation can be described by the behavioral models explained in Chapter 2. For the case of a TX, it is common to use a nonlinear model only for the PA for simplification since it covers the most dominant nonlinear effect [22–25].

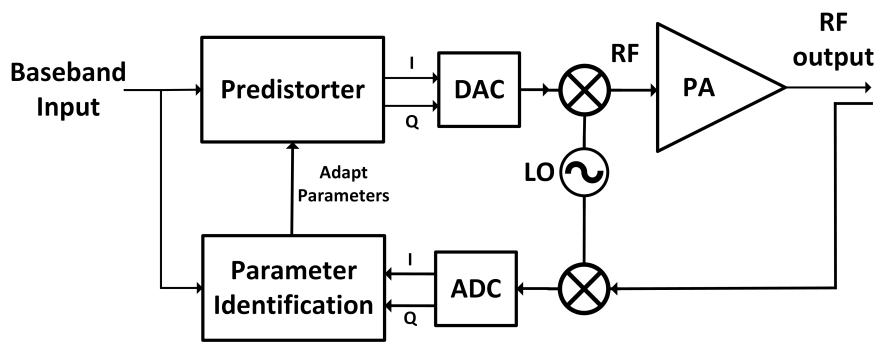

Figure 3.4: Block diagram of the digital predistorter control loop for linearization of a PA.

One method to identify the parameters of the predistorter to achieve "linear response" is, using a feedback architecture as the basis of the predistorter system as seen in Figure 3.4. The output of the PA is down-converted and demodulated and then converted into I and Q data streams using an analog-to-digital converter (ADC). Finally, the outgoing I/Q data is compared to the data from the ADC, which is adjusted by the pre-distortion algorithm [14]. After the combined action of the DPD and the PA through a control loop, we expect the output signal to be linearly scaled version of the input signal.

3.2.2 Analog Predistortion

Analog predistortion is realized by cancelling the effects of distortion by using analog components. They are frequently used in space applications and hand-held communication devices, where power consumption is important [14]. The nonlinear compensation is created using a low order function when compared to DPD due to challenges related to circuit complexity for the creation of higher order polynomials and memory implementations. APD can potentially provide wider bandwidths, lower cost and simpler structure [45,46]. For wireless

communications including mm-wave, with baseband APD, it is possible to implement wideband linearization without the need of high signal processing power of DPD.

There are different ways to implement analog predistortion including baseband or RF [45–48]. In particular, when analog predistortion is realized in baseband, the carrier frequency becomes a freedom of choice, similar to the DPD case, since the baseband signal is upconverted by the TX. In this thesis, this specific feature is used to linearize an E-band direct conversion transmitter as it will be shown in Chapter 4.

3.3 Parameter Identification

An important step of behavioral modeling is model parameter identification. The model of the PA or the TX depends on the type of data it used in the identification process. The parameter estimation process needs to be carefully handled since most of the black box models suffer from uncertainty during modeling [20]. Due to the statistical nature of measured communication signals, most Volterra-based models can be identified with a least squares estimate. Depending on the model complexity, this procedure may need an iterative process.

Parameter identification for digital and analog predistorters may require different approaches. Especially for APDs, this process depends of extensive characterization of the device.

3.3.1 Parameter Identification in Digital Predistortion

The DPD should implement the inverse function of the PA nonlinearity. In order to do this task, the coefficients of the model of the PA should be found from the input-output pairs of the PA, see Fig. 3.4. Then the nonlinear PA function should be inverted to obtain the predistorter coefficients. This inversion can be problematic especially when memory effects are included [14]. Hence, various approaches including direct learning architecture [49], pth-order inverse technique for Volterra series [50] and indirect learning architecture [51], are proposed in the literature.

Direct learning architecture presents slow convergence. While the Volterra series has a direct formal inverse, pth-order inverse technique requires calculation of too many coefficients and has some stability problems [50]. This problem can be overcome by identifying the inverse PA model directly. This approach is called indirect learning architecture (ILA). In this thesis we focus on ILA, and apply it to both a PA and a TX, hence this technique will be explained next.

Indirect Learning Architecture

Indirect learning architecture is one of the most widely used techniques to identify the digital predistorter parameters, first introduced in [51] and further improved in [52]. The block diagram of the ILA architecture is presented in Figure 3.5. The architecture is well established with different implementation variants [53, 54]. In the classical variant, the initial training begins by setting the 'Predistorter' block to the identity transformation such that $u(n) = x(n)$.

The 'Postdistorter' block has the scaled version of the measured PA output, $y(n)/G$, as the input, where G is the desired gain of the PA. The 'Postdistorter' block has the output $u'(n)$, which is the output of a nonlinear model with memory. Here, the 'Postdistorter' has the approximated predistorter model parameters. The post-distorter coefficients are copied to the predistorter. Using $u(n)$ and $y(n)$, the predistorter is identified in post-inverse configuration by minimizing the magnitude of the error signal $e(n) = u(n) - u'(n)$. Finally the model coefficients that minimize $e(n)$ are copied to the predistorter and the input $x(n)$ is predistorted. In order to minimize the error magnitude between the model prediction and the measurements for the postdistorter, least squares estimation algorithm is commonly used. Hence, the overall error is minimized in the iterative control loop that the ILA architecture represents.

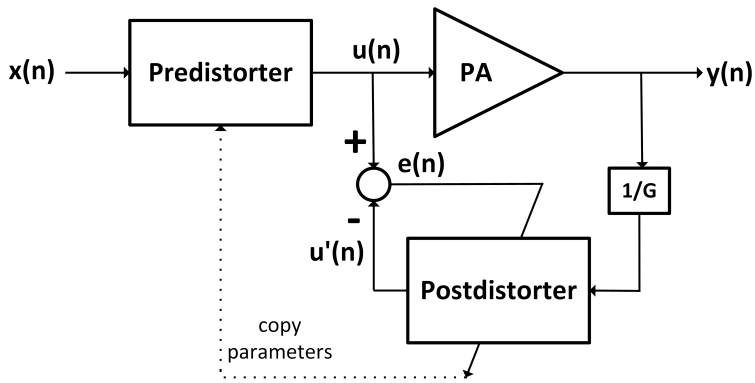

Figure 3.5: Block diagram showing the working principles of indirect learning architecture.

3.3.2 Parameter Identification in Analog Predistortion

In analog domain, predistorter parameters are identified by complete characterization of the device for all possible polynomial order combinations. Depending on the complexity of the circuit, it is possible to use varying sizes of LUTs. For example, a diode based APD can be represented by far less number of parameters when compared to a Gilbert cell analog multiplier based high order APD. The analog predistorter used in this thesis is a 7th order complex memoryless polynomial predistorter with 8 coefficient controllers, see [Paper B] for details. To be able to find the parameters of such a predistorter, a grid search needs to be performed, where each controller voltage is swept within their corresponding limits. As it will be presented in Chapter 4, even the full range of parameters for such an APD may fall short when compared to a DPD.

3.4 A General Framework for Evaluation of Predistorters

We use the framework introduced in this section to study transmitter linearization and performance improvement using different test signals. A block diagram of the framework used to analyze the transmitter performance is

shown in Fig.3.6, which was adapted from [Paper A]. The main blocks of the framework are the predistorter, the nonlinear DUT (PA or a transmitter), and post processing. These blocks are controlled by several different parameters. For the test signal, the inputs can be the modulation order of the signal, its amplitude and bandwidth. The predistorter can have different polynomial orders, hence coefficients. The nonlinear DUT can have different measured input-output pairs for different frequency points. Finally the resulting signal is post-processed to acquire important metrics such as EVM, PAE, etc.

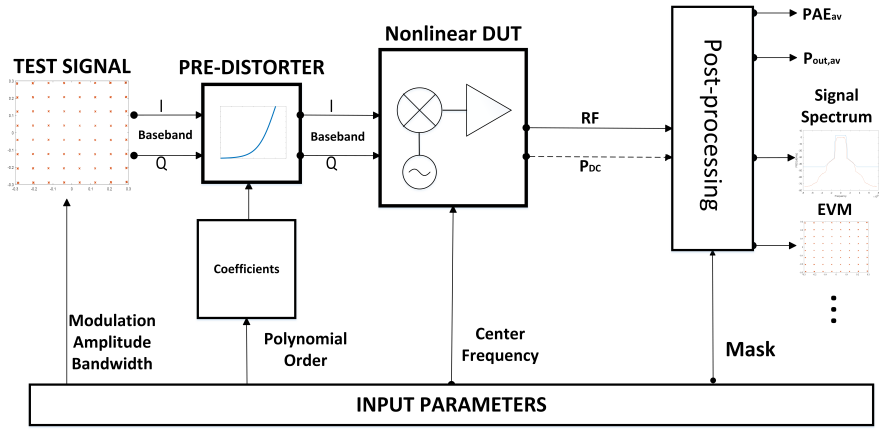

Figure 3.6: Block diagram of the linearization process of the nonlinear DUT.

3.4.1 Test Signals

In Fig. 3.6, the block diagram illustrates the input-output relation of a modulated signal which is used to predict the signal spectrum and efficiency of the tested system. In the scope of this thesis, QAM signals of different orders are used and filtered with a raised cosine filter. Within this framework, it is also possible to use other types of signals such as single or multi-tone sinusoidals. The communication signal is represented by randomly created information bits and then modulated using a wireless communication signal at baseband. This signal is then sent to the predistorter.

3.4.2 Predistorter

The input parameters for predistorter block in Fig.3.6 includes control options such as the polynomial order and polynomial coefficients of an APD or a DPD. Here, the predistorter is located before the TX. With this framework, it is possible to implement a linearization technique in the analog or digital domain. This framework will be used as the basis for linearization of a mm-wave PA and an E-band TX using both digital and analog predistortion in Chapter 4.

During the implementation, the first step is to numerically find a polynomial where the linearization is optimal, using the models of both the predistorter and the nonlinear DUT. Average input power level of the test signal is adjusted so that the DUT is pushed to its nonlinear region while meeting the spectrum mask

requirements. Using simulations, the polynomial coefficients of the predistorter, either in analog or digital domain are found, where the most improvement was achieved. These coefficients can later be used as a starting point for the measurement setup of the DUT. Later in Chapter 4 we show that, this starting point needs to be adjusted in its neighborhood to fine tune for best performance.

3.4.3 Post Processing

One of the important standard that communication signals need to follow is the spectrum emission of the transmitted signal. For different signal modulation types and orders, different spectrum emission masks are used to test whether the signals follow these standards or not [7]. In a device test environment, the spectrum emission performance is tested by gradually increasing the input power level until the mask requirement is breached.

At the post processing block of the framework, other device metrics are also calculated. For example, the RF signal and the DC power models and characteristics of the predistorter and the transmitter blocks are used to calculate average output power ($P_{\text{out,av}}$), average power added efficiency (PAE_{av}) and error vector magnitude (EVM). These metrics will be exemplified in Chapter 4.

While the predistorter block handles the nonlinear effects, linear intersymbol interference is handled by the post processing block by performing linear equalization to the output data. The equalization process implemented in this thesis consists of positive and negative delay elements centered around $t = 0$.

This chapter summarized digital and analog predistortion techniques and their applications. These techniques will be applied to the models of a PA and a direct conversion TX for linearization and trade-off analysis in the next chapter.

Chapter 4

Predistortion of mm-Wave Systems

Nonlinearities in RF systems cause signal degradation. Due to intermodulation distortion, the signal experiences spectral regrowth and in-band distortion. However, designing a communication system with only linearity in mind, forces engineers to use class A power amplifiers. These PAs lack the efficiency merits at backed-off power levels that communication systems want to benefit from. On the other hand, high efficiency PAs, like other classes or more advanced architectures such as Doherty, suffer from increased nonlinearity. Predistortion is the most regularly used technique to linearize such devices, so that the communication is established both linearly and efficiently.

In previous chapters, characterization and modeling methods that can be used for PAs and TXs were identified. In addition, a framework was proposed for linearization of these devices. In this chapter, firstly the trade-offs arising from the level of predistorter complexity are analyzed for different PA classes using this framework. Second part of this chapter is dedicated to linearization of an E-band TX with a baseband APD.

4.1 Trade-offs in a Linearized mm-wave Class AB Power Amplifier

We now investigate the interdependency of the performance of a linearized class AB PA from various perspectives, including predisorter complexity, linearity and efficiency. This section provides an overview, whereas a more detailed treatment is presented in [Paper A].

As the most power-consuming part in the transmitter, highly efficient PA designs are always sought after. These kinds of designs require several considerations at the same time, such as power consumption, noise figure, gain, bandwidth, stability, etc. For communication systems, low power consumption and efficiency is of interest to decrease excess heat and increase hands-on time for mobile devices, and operating cost and CO2 emissions from mobile infrastructure installations. In order to successfully send and receive a communication signal, the PA should also have flat response inside the bandwidth of

operation to minimize memory effects. The efficiency and linearity are usually contradicting metrics and dependent of the PA class.

In this section, the level of complexity of the predistorter needed for a PA to perform linearly is investigated. To investigate the trade-offs, the framework introduced in Section 3.4 is used on a class AB PA that operates between 26.5-31.5 GHz. This PA is biased with different gate voltages, which spans a range that covers class A to class C.

4.1.1 Methodology

Analysis of the aforementioned trade-offs require a certain set of information, which usually starts with device characterization. The device used here is a mm-wave PA with a center frequency of 29 GHz. At the end of the characterization process, AMAM and AMPM characteristics are found. This is repeated for different gate biases to test different PA classes. For each data point, DC power characteristics need to be recorded to calculate the efficiency later on. The PA is then linearized using a predistorter, where the complexity is controlled through its polynomial order. Here, for each PA class, the linearity improvement is observed for a certain level of predistortion complexity. Linearity level is tested by applying a spectrum emission mask to the output signal spectrum and comparing the average output power at the mask limit for each case. Since efficiency response changes for different PA classes, average PAE after predistortion is also of interest for these cases.

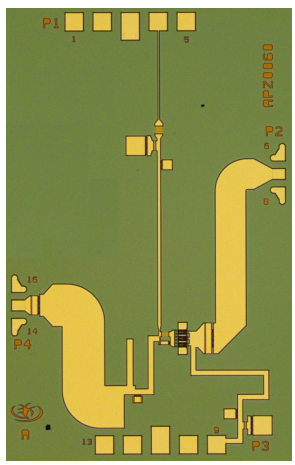

Figure 4.1: The Ka band MMIC PA used for the trade-off analysis in [Paper A].

4.1.2 Characterization and Modeling

The MMIC circuit was fabricated by Win Semiconductor using their pp1010 pHEMT process. A photo of the chip can be seen in Figure 4.1 . The PA tested uses a single $6x50\mu m$ transistor and optimized for class AB operation. This results in a small signal gain of 8 dB at a V_{DS} of 3.3V. To record the response of different classes, V_{GS} is swept from -0.9V to -0.4V. The block diagram of the measurement setup can be seen in Figure 4.2. The measurements are performed

using a nonlinear VNA, PNA-X N5247A by Keysight. It is noteworthy to mention that the presented measurements are performed at a single frequency of 29 GHz. The reason for the approach is that we are not interested in any memory effects during the trade-off analysis.

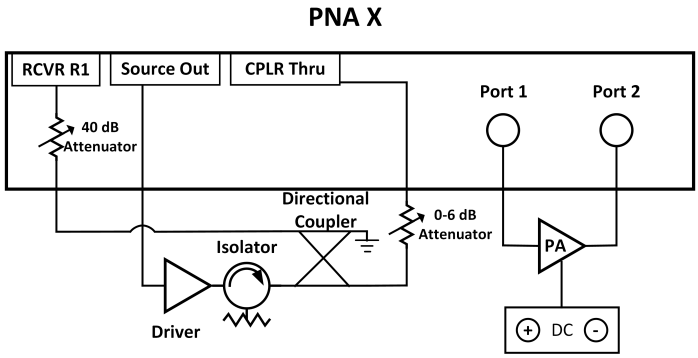

Figure 4.2: Block diagram of the measurement setup for the PA characterization

The measured saturated power level of the PA is 23.5 dBm, which requires an input power level of 20 dBm for class C operation. The network analyzer has a limited power source range, hence a driver amplifier is used to reach to this power level requirement before port 1 of the PNA-X as seen in Figure 4.2. The calculated AMAM and AMPM responses using the performed 2-port S-parameter measurements at 29 GHz can be seen in Figure 4.3. From the figure, we can see that the flat gain response at class A operation at -0.4V gradually increases the nonlinear effects when we go towards class C operation at -0.9V. We can observe a similar response for the phase conversion.

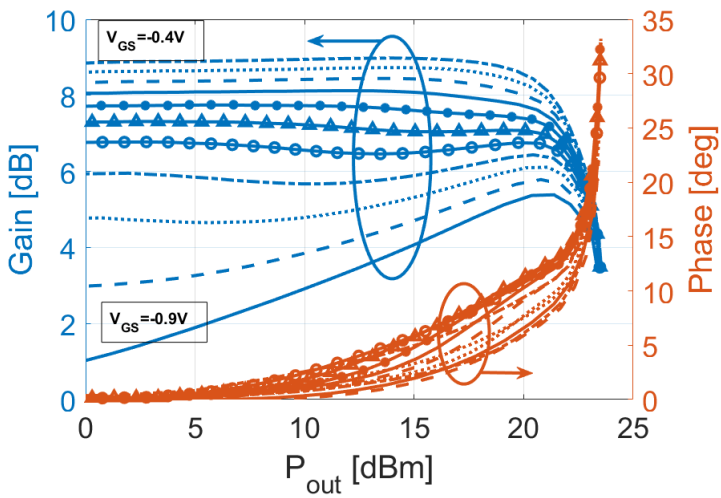

Figure 4.3: Measured AMAM and AMPM characteristics of the PA at 29 GHz

An important metric we can calculate using the AMAM/PM characteristics and the collected DC consumption values is the PAE. The PAE response

with respect to the output power can be seen in Figure 4.4. Here we can observe that, when the output power level is backed off to 15 dBm, the PAE changes significantly between classes. For example, it increases from 11.5% at $V_{GS} = -0.4$V to 18% for at $V_{GS} = -0.8$V. When the gate-to-source voltage is decreased further towards pinch-off, efficiency decreases again due to low gain at this power level.

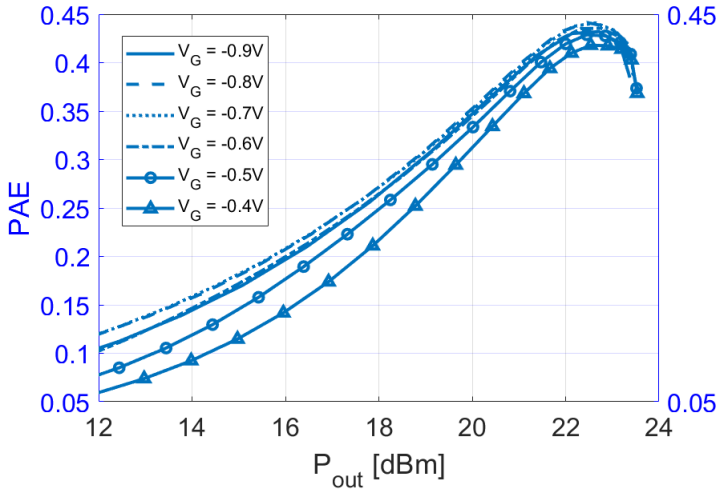

Figure 4.4: Calculated PAE response of the PA at 29 GHz

The model of the PA depends solely on the measured AMAM and AMPM data during the characterization. The quasi-static PA model was created at a single frequency. For each input power level, there exists a corresponding output level which was found by interpolating between the measured points. This model assumes that the PA characteristics stay the same in the signal bandwidth while the remaining dominant nonlinear effects are included.

4.1.3 Trade-offs Between Complexity, Linearity and Efficiency

Using a 64 QAM signal with 192 MS/s and 10000 symbols, the PA is tested with the framework proposed in a computer simulation environment. Firstly, the signal is applied to the PA only and gradually increased power level is compared to a 250 MHz spectrum emission mask for different bias points until it is breached. Then a predistorter with 3rd, 5th and 7th order polynomials are applied to the PA and then compared to the same spectrum emission mask. Here, the predistorter parameters are identified for different power levels using ILA, where the coefficients are found using a least square method.

Figure 4.5 presents average output power at the mask limit for different gate biases. With the implementation of predistortion, some level of interference suppression is expected at adjacent channels that is caused by compression at high power levels. Here, we can see that the average output power is improved to some extent for all bias levels when linearization is applied. When we go

towards class C region, where the nonlinearity is higher, the improvement increases for higher order polynomials. The gap between 3rd and higher order polynomials decrease when the PA is already in its linear response region such as when $V_{GS} = -0.4V$. At this bias point, the predistortion performance is also minimal when compared to for example class B and C operation. This difference is around 1dB vs >6dB improvement at$V_{GS} = -0.4V$ and $V_{GS} = -0.8V$, respectively. Another interesting result is that the power level after linearization stays relatively constant when $V_{GS} > -0.7V$ for different predistorter complexities.

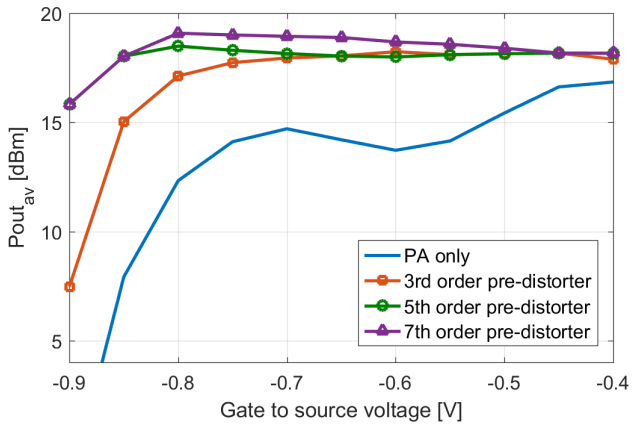

Figure 4.5: Average output power for different bias points and different predistortion polynomial order at the spectrum mask limit

Figure 4.6 presents PAE levels at the spectrum emission mask limit when 3rd, 5th and 7th order predistortion polynomials are used for different gate biases. The average PAE has a peak value and the largest improvement at $V_{GS} = -0.8V$, where it can be considered as class B operation. At this point there is a 3dB average output power improvement between 3rd and 7th order predistorters, which translates to 12% improvement in PAE. Here, another interesting result is at $V_{GS} = -0.4V$; there is no significant difference in PAE level for 3rd, 5th and 7th order polynomials. There are two main reasons for this result. Firstly, the compression profile of the PA at this bias point can be compensated for successfully by using a 3rd order polynomial. Also, the device is already operating close to its output limit, so there is not much improvement room in terms of power level.

Figure 4.7 presents the power spectral density of the output signal with and without predistortion. The point of operation is chosen to be $V_{GS} = -0.7V$ and output of the PA is set to a constant value of 17.8 dBm to exemplify the effect of different polynomial orders. For this specific bias point, we can easily distinguish the 3rd, 5th and 7th order predistortion when compared to the PA only case.

In this section, we have investigated the trade-offs between the linearity, output power, efficiency and complexity for a mm-wave PA. We have shown how much improvement is achieved in average efficiency and output power for different PA classes. Another result is that even a 3rd order predistorter can

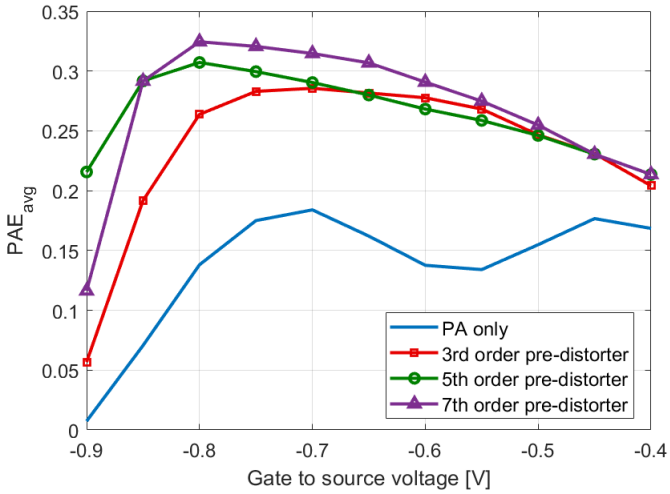

Figure 4.6: Average PAE for different bias points and different predistortion polynomial order at the spectrum mask limit

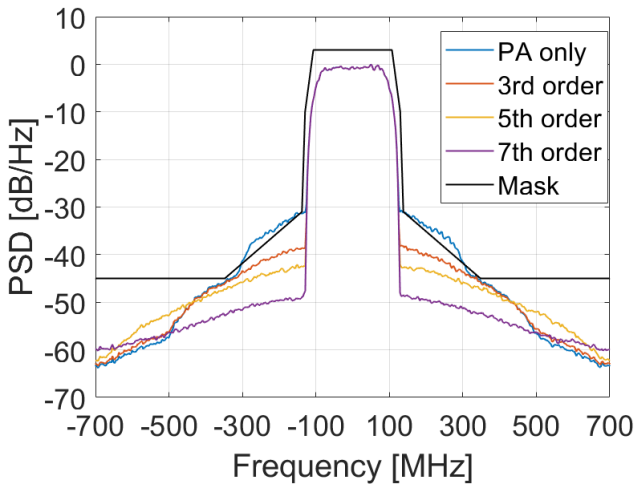

Figure 4.7: Comparison of the mask and the power spectral density of output signal without pre-distorter and with 3rd, 5th and 7th order pre-distorters for constant power level of 17.8 dBm. For this specific case, a V_{GS} of $-0.7V$ is used as the operation point.

give significant efficiency improvement for certain PA classes under spectrum mask constraints.

4.2 APD Linearization of an E-band Transmitter

In this section, we present the linearization of a direct conversion transmitter using an analog predistorter. This section provides an overview, whereas further

details can be found in [Paper B].

The APD circuit, shown in Figure 4.8, is implemented in a commercial 130 nm SiGe BiCMOS process. Gilbert cell analog multipliers are used in the predistorter chip, which measures approximately $900\mu m$ by $600\mu m$. The chip aims to correct AM-AM nonlinearities as well as AM-PM nonlinearities by implementing a 7th order complex polynomial.

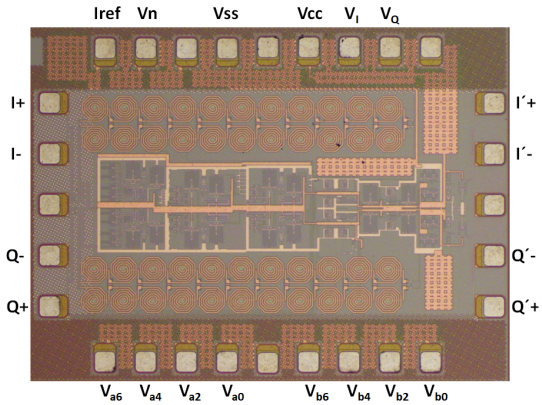

Figure 4.8: Photo of the APD chip. Bias and controller voltages are marked on the pads.

The transmitter block diagram and the chip's photo on an evaluation board (EVB) are provided in Figure 4.9. The chip has its own integrated $\times 6$ LO multiplier in addition to a VGA, IQ modulator and PA. Through the EVB, SMA, WR12 waveguide and DC connector interfaces are used for measurements. Further properties of the TX chip are presented in [Paper B]. The TX's characterization results can be found in Section 2.3.

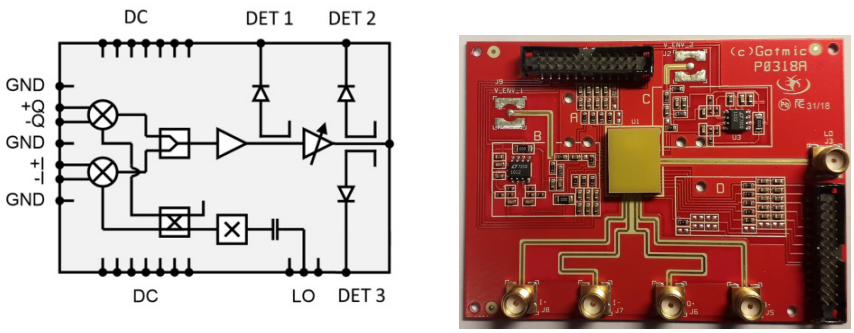

Figure 4.9: Block diagram (left) of the TX and its photo when mounted on an evaluation board (right).

First the methodology to linearize the TX is summarized. Then, the characterization and modeling of the APD is presented. Using the models of the APD and the TX, the linearization process is simulated. Finally, using the information gathered from the simulations, a measurement setup is used to linearize the TX using the APD.

4.2.1 Methodology

The framework followed in this section is explained in Section 3.4. We start by characterization of the TX (given in Section 2.3) and the APD circuit that is available. The measured data is then used to model both of the devices following the procedure in Section 2.2.3. The models are then used to simulate the predistorter system by the use of a test signal, a set of predistortion coefficients and recovery of the output signal. Here, the APD is connected to the input of the transmitter. The metrics such as PAE and average output power level at the spectrum mask limit is achieved using post-processing. The best results of these simulations are then used as a starting point for setting up the APD circuit to linearize the E-band TX.

4.2.2 Characterization and Modeling of the APD

The APD chip used for the linearization of the TX implements a 7th order, complex memoryless polynomial predistorter with differential I and Q channels. A more detailed function implementation and hardware specification information can be found in [Paper B]. The APD chip by itself can provide a maximum linear output power level of -10 dBm with a 100Ω differential load. To push the TX to its P1dB point, we need at least 8 dBm at its input. To solve this problem, we cascaded an additional amplification stage at the output of the APD chip, which was sufficient to push the signal level before the TX to 10 dBm.

Figure 4.10 presents the block diagram of the measurement setup for the characterization of the APD, including the additional amplification stage. The predistorter has a total of 11 controller voltages to manipulate the signal according to our needs. Hence, the characterization would normally require a complete voltage sweep combinations of all of these controllers. The predistorter's 5th and 7th order function generators caused a low frequency oscillation which is not easily fixable. 1st and 3rd order function controller voltages for I and Q channels has a full operation range of 0 to 100mV, even when 5th and 7th order generators are turned off. We refer to these voltages as V_{a0}, V_{a2}, V_{b0} and V_{b2}, which control 1st and 3rd order coefficients of I and Q nonlinear channels, respectively. Hence, the complete characterization requires more than 10000 polynomial coefficient combinations, when 10mV intervals are used.

The characterization is performed by using a 256 QAM, 10000 symbol test signal with a root raised cosine filter roll off factor of 0.3 and symbol rate of 192MS/s. The signal is provided by an Agilent 81180B arbitrary waveform generator and recorded in time domain with a LeCroy Waverunner 640Zi oscilloscope with 4 channels, as shown in Figure 4.10. A 21 tap linear equalizer is implemented to the recorded signal to handle the linear distortion due to mismatch and reflections and dynamical effects in the APD circuit. In Figure 4.11, we present the functionality of the APD for 1st order and 3rd order responses using two recorded constellation diagram examples.

The modeling of the APD closely follows that of the direct conversion TX given in Chapter 2.

Ideally for the APD, if we ignore the memory effects in the circuit, M should be zero. The ideal input-output relationship of the APD has the following

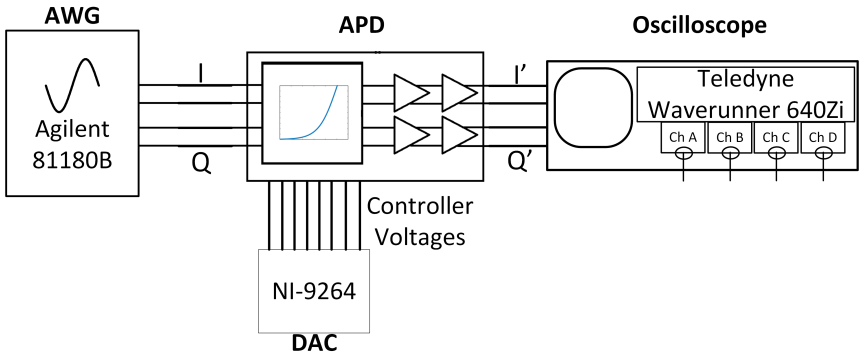

Figure 4.10: Measurement setup for predistorter characterization.

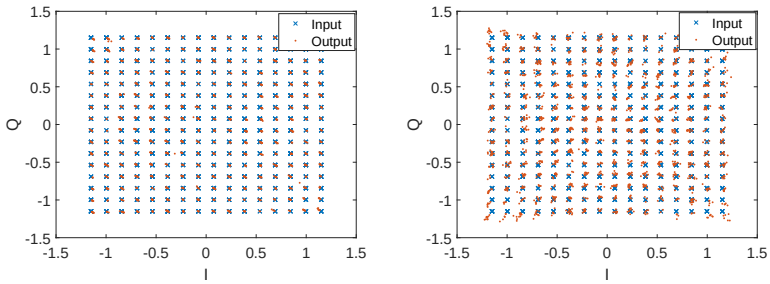

Figure 4.11: Constellation diagrams at I/Q output for $[V_{a0}, V_{a2}, V_{b0}, V_{b2}] = [100, 0, 10, 0]$ mV (left) and $[100, 0, 50, 0]$ mV (right).

form:

$$y = \sum_{p=0}^{3} (a_{2p} + jb_{2p})(x_I + jx_Q)|x_I + jx_Q|^{2p} \tag{4.1}$$

Here, $x = x_I + jx_Q$ and $y = y_I + jy_Q$ are baseband representations of the input and output signals of the APD, respectively. In the APD circuit, a_{2p} and b_{2p} values in (4.1) are controlled by V_{a2p} and V_{b2p}, respectively. To achieve a good agreement between the measurements of the real circuit and the model, we used $M = 3$ and $P = 5$ to include non-ideal characteristics such as I/Q imbalance, memory and higher order nonlinear terms. Figure 4.12 presents a comparison of the dynamic response between measured and the modeled signal with an NMSE value of -28dB.

4.2.3 Model Simulations

After characterization and modeling of both the APD and the TX, we can create a simulation to test the cascade connection of the APD and the TX. Similar to the linearization of the mm-wave PA shown in Section 4.1, a QAM signal with 10000 symbols and 192 MS/s is increased in power until the output signal breaches the spectrum mask. The simulations are performed with different controller voltage values within the range of operation of the APD. The purpose of using such a large set of voltage values is finding the settings that give the

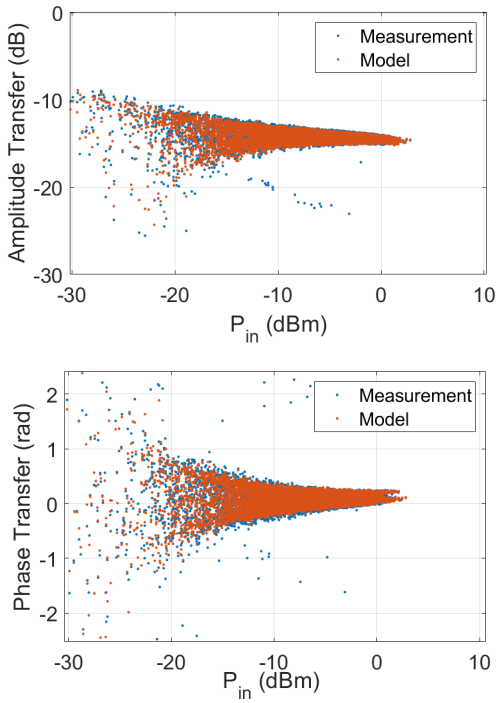

Figure 4.12: Comparison of dynamic amplitude and phase transfer from input to output of the measurement and the model. The signal used has a symbol rate of 192MS/s. The controller voltages used for the specific case are $V_{a0} = 90$ mV, $V_{a2} = V_{b0} = V_{b2} = 0$.

best linearization performance. Hence, we want TX to operate at a higher output power at the spectrum mask limit when the APD is active.

At the mask limit, average output power, EVM and PAE is calculated for QPSK, 16QAM, 64QAM and 256QAM signals. For each modulation order, different levels of improvement in average output power is obtained at the mask limit. A comparison of these power levels at the spectrum mask is provided for different modulation orders in Table 4.1.

Table 4.1: Average output power levels at the spectrum mask limit for different modulation orders with APD, with DPD and without using a predistorter. For each modulation order, a different spectrum mask is implemented for a signal with 250 MHz bandwidth [7].

Average output power at mask limit (dBm)				
	QPSK	16QAM	64QAM	256QAM
w/o Predistortion	21.17	19.12	15.70	15.35
with APD	21.44	19.58	17.45	16.80
with DPD	21.91	19.95	18.90	17.30

We observe the best improvement when compared to the case without any

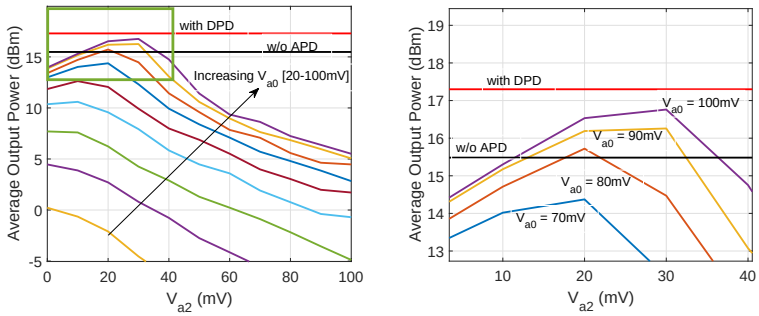

Figure 4.13: Average output power level at the spectrum mask limit using the APD for different V_{a0} and V_{a2} combinations, compared to a 3rd order digital predistortion and without predistortion (left). The same figure, zoomed in to the area where the APD improves the output power of the TX at the mask limit (right).

predistortion, is seen for 64QAM and 256QAM signals. For 16QAM and QPSK signals, the intermodulation requirement of the spectrum masks is significantly relaxed and the enhancement in average output power becomes marginal.

We also replaced the model of the APD with a DPD of the same order to better understand the performance of the APD. For parameter identification, ILA is used for a 3rd and 5th order DPD implementation. During this implementation, we observed increasing the DPD order from 3rd to 5th only adds 0.03dB to the average output power for this TX model. Figure 4.13 shows the average output power at the spectrum mask limit for different V_{a0} and V_{a2} combinations of the APD compared to a 3rd order DPD, and the case without predistortion. From the figure, we can observe that only a small set of V_{a0} and V_{a2} combinations results in improving the original TX, while the DPD results in the best performance.

4.2.4 Measurement Testbed and Results

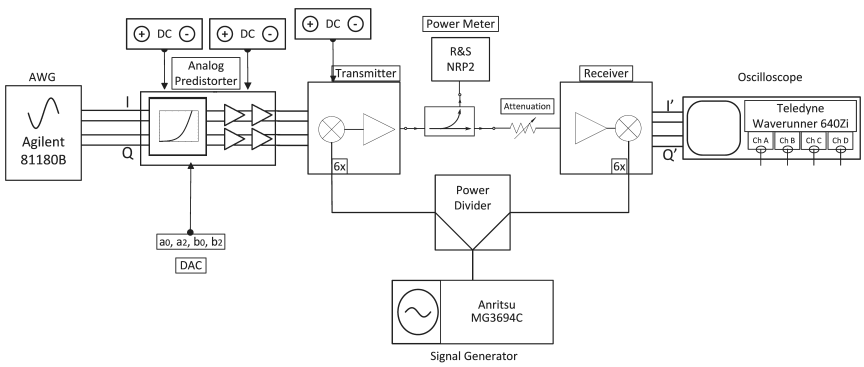

Figure 4.14: Block diagram of the measurement setup for linearization of the transmitter using the analog predistorter

A block diagram of the measeurement setup for linearization of the TX using the APD can be seen in Figure 4.14. Here, QAM modulated differential

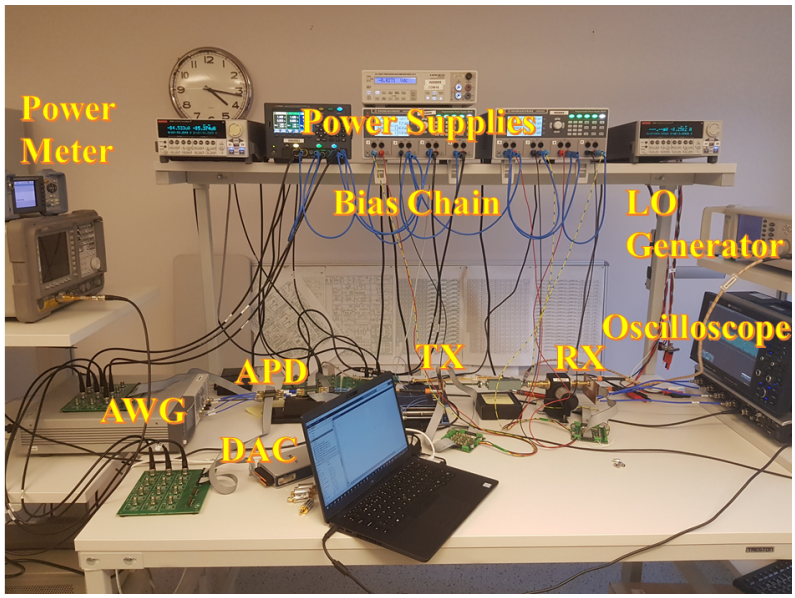

Figure 4.15: Photo of the measurement setup for TX linearization using analog predistortion.

baseband I and Q signals are sent from the AWG to the APD. The function required to linearize the TX is approximated using the estimated coefficient controller voltages in the previous section, $[V_{a0}, V_{a2}, V_{b0}, V_{b2}]$. After the linearization, resulting TX output signal is downconverted to baseband using the RX circuit. Using the oscilloscope, the differential I and Q baseband output signals are then recorded in time domain. The time domain signal is further processed to obtain the signal spectrum, which is compared to the spectrum emission mask. Average output power is recorded using the power meter. A photo of the complete measurement setup can be seen in Figure 4.15.

The voltage values predicted by the modeling technique presented in the previous section are $[V_{a0}, V_{a2}, V_{b0}, V_{b2}] = [100, 30, 0, 20]$ mV. These values resulted in a worse power levels at the mask limit than the model prediction. The main reason for the performance drop is due to the LO leakage level. After the application of LO cancellation, the signal spectrum has become clear of LO leakage.

To find a suitable spot for improved linearity, several iterations were performed. The best combination for the controller voltages are found to be $[V_{a0}, V_{a2}, V_{b0}, V_{b2}] = [100, 38, 0, 25]$ mV with LO cancellation, which is very close to the model prediction. Next, the TX is tested with and without an APD at average output power level of 16.8 dBm and their spectra is compared to that of the DPD at the same power level. The resulting spectra, compared to the spectrum mask are presented in Fig. 4.16.

Here, the DPD is realized by connecting the AWG directly to the input of the TX and the coefficients for the polynomial are extracted from the simulations and used to shape the modulated signal. At the mask limit, an average power of 17.5 dBm is obtained, but the power level is backed-off to 16.8

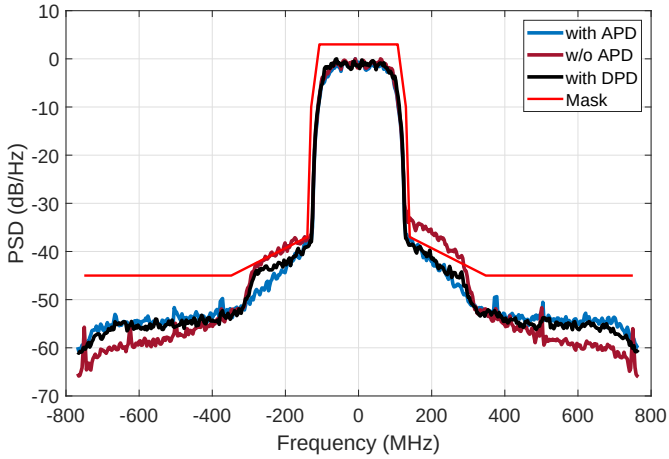

Figure 4.16: Comparison of the measured output spectra of the TX with and without the APD after linearization. Average output power is 16.8 dBm for both cases for direct comparison. For benchmark, measured spectrum with DPD is shown for the same output average power level.

dBm to directly compare it to the APD. It is shown that, the APD successfully linearizes the TX. The TX before the linearization had an EVM level of 2%. The APD has degraded the EVM level to 2.3%, while gaining 1.5dB average output power. The DPD's linearization performance results in slightly more output power, while the APD has overall better shoulder suppression for the used set of coefficients.

In this section, we have linearized an E-band transmitter using an analog predistorter. Firstly, APD and the TX were characterized individually. Then, the resulting models were used to model the mapping from the dynamic baseband input to RF output of the overall system consisting of cascade combination of the APD and the original TX. Using this model, full system performance is estimated by simulations and optimal control voltage settings of the APD are identified. These voltages are then used as a starting point for the APD linerization setup. The measurement results show that when used in this setup, the APD increases the average output power of the TX at the spectrum mask limit from 15.4 dBm to 16.7 dBm, corresponding to a %35 increase.

Chapter 5

Conclusions

In order to optimize the performance of modern communication systems, design of efficient power amplifiers with linear operation region is needed. In this thesis, we have addressed this challenge using predistortion based linearization. We have proposed a comprehensive framework for evaluation of predistorters. The framework enables us to investigate the trade-offs between linearity, efficiency and predistorter complexity systematically. The proposed framework is implemented for two applications using a practical communication system setup and successful linerization is illustrated with measurements: i) a mm-wave PA using digital predistortion, and ii) an E-band TX using an analog predistorter.

In the first part, we have focused on the mm-wave PA. We have investigated the effect of predistortion complexity and PA class on the optimum trade-off between linearity and power efficiency. Our results quantified the substantial impact of the PA class and the predistorter complexity on the output power and the power added efficiency. It is illustrated that for the considered PA, class A and AB nonlinearities could be compensated by a 3rd order predistorter with diminishing returns with higher order predistorters. On the other hand, for class B and class C operation, higher order predistortion was needed, which gave both considerably higher average output power and power added efficiency at the spectrum mask limit compared to 3rd order predistorter.

In the second part of the work, we targeted an E-band direct conversion transmitter using the same framework. This extensive work also covered characterization and modeling of the APD and the TX. Using the created models, a simulation study is performed with communications test signals with varying modulation to estimate the performance of the cascade combination of the two devices. We used an analog predistorter to increase the output power while satisfying the spectrum emission mask and compared the results to the equivalent digital predistorter with same order and no memory. The simulations covered QPSK, 16QAM, 64QAM and 256QAM test signals. These simulations showed that a significant improvement in output power at the mask limit is obtained for the latter two modulation schemes, when a predistorter is used (APD and DPD) compared to the case where there is no predistorter. The estimated controller voltages from these simulations are then used as a starting point for the APD linearization setup. Similar levels of improvement with

the simulations are achieved after fine tuning of the controller voltages during the measurements, demonstrating the practical viability of the APD setup. In particular, our experiments demonstrated that the analog predistorter can successfully increase the output power by 35% (1.3 dB improvement) while satisfying the spectrum emission mask.

The nonlinearities mitigated by the presented set-up are among the central factors which can degrade the performance of the transmitter, and hence the overall communication system. This thesis provided a systematic framework to evaluate the performance trade-offs between linearity, efficiency and predistorter complexity; further supporting future systematic studies. Moreover, increased power output with predistortion was demonstrated, which suggests higher SNR, and hence higher data rates. With the proposed framework and its successful demonstration, this thesis contributes to addressing the need for higher data rates in modern communication systems.

5.1 Future Work

The work in this thesis can be further followed up on several tracks. These possible research directions are summarized below:

Advances in the APD design: The output power level of the APD used in this work is low compared to the power level required for direct compensation of the targeted TX. Hence, a driver baseband amplifier chain is used to satisfy the power budget of the system. This causes severe limitations in function generation capabilities of the APD, since the output is modified before the TX. Another drawback of using driver amplifier chain to boost the APD level is the fact that the noise floor is also boosted, which in turn causes a loss in dynamic range. Hence, it is imperative to improve the APD design for better function generation capabilities and dynamic range.

Another improvement for the APD design would be inclusion of memory effect compensation. With digital predistortion, memory polynomials are used for the compensation of some of the unwanted dynamic effects for broadband signals. A more complicated APD design can mimic this effect to some extent and thus enable APD for larger bandwidths.

The APD used in this work was designed for up to 7th order polynomial generation, but could only generate 3rd order functions in a stable manner. As shown in this work, higher than 3rd order polynomials are needed for improving the performance of PAs with more complicated AMAM/PM responses. Hence, design of APD with higher order function generation capabilities is desirable.

Towards a self correcting system: The measurement setup for TX linearization presented in this work can be extended using a feedback loop in order to automatically adapt to changes in the system. One example for possible changes in the system is the temperature changes at different power levels, which affect the amplitude and phase transfer profile. Another would be to make the TX adapt to changes in the signal statistics when the modulation order changes. When these changes occur, they need to be compensated by a new set of predistortion coefficients in order for the system to operate optimally. Hence, it is of interest to design a feedback mechanism to achieve this compensation automatically.

Design choice between APD and DPD: An interesting research question is a-priori determination of suitability of APD and DPD for a particular application. Although DPDs are quite popular, APDs provide a viable alternative, as illustrated in this thesis. Given the potential benefits of APDs, further studies on APD performance and clear understanding of performance trade-offs for APD and DPD based linearization techniques are needed.

Another related research direction is combination of DPD and APD in the same system. It has been shown in [38] that the APD and the DPD can be used to compensate for different nonlinearities of the DUT, each with their own strengths. Design of a system that brings these strengths together in an optimal manner and investigations of the efficiency, linearity and complexity trade-offs therein is a promising research direction.

Bibliography

[1] R. N. Mitra and D. P. Agrawal, "5G mobile technology: A survey," *ICT Express*, vol. 1, no. 3, pp. 132 – 137, 2015.

[2] M. Zeng, A. Annamalai, and V. K. Bhargava, "Recent advances in cellular wireless communications," *IEEE Communications Magazine*, vol. 37, no. 9, pp. 128–138, 1999.

[3] R. L. Pickholtz, R. Prasad, and H. Lee, "Special Issue on IMT 2000," *Journal of Communications and Networks*, vol. 2, no. 1, pp. 1–4, 2000.

[4] S. Ohmori, Y. Yamao, and N. Nakajima, "The future generations of mobile communications based on broadband access technologies," *IEEE Communications Magazine*, vol. 38, no. 12, pp. 134–142, 2000.

[5] "This is 5G," Ericsson AB, Tech. Rep., May 2020.

[6] "Ericsson Mobility Report," Ericsson AB, Tech. Rep., June 2020.

[7] "Fixed radio systems; characteristics and requirements for point-to-point equipment and antennas; part 2-2: Digital systems operating in frequency bands where frequency co-ordination is applied; harmonized EN covering the essential requirements of article 3.2 of the R and TTE directive," *ETSI EN 302 217-2-2 V2.2.0*, 2013. [Online]. Available: http://www.etsi.org

[8] "Multiple Gigabit Wireless Systems in Frequencies Around 60 GHz," International Telecommunication Union, Tech. Rep., November 2016.

[9] "Application For Approval For Orbital Deployment and Operating Authority For the SpaceX Gen2 NGSO Satellite System," Federal Communications Commission, USA, Tech. Rep., June 2020.

[10] P. Wang, Y. Li, L. Song, and B. Vucetic, "Multi-gigabit millimeter wave wireless communications for 5G: from fixed access to cellular networks," *IEEE Communications Magazine*, vol. 53, no. 1, pp. 168–178, 2015.

[11] C. Dehos, J. L. González, A. D. Domenico, D. Kténas, and L. Dussopt, "Millimeter-wave access and backhauling: the solution to the exponential data traffic increase in 5G mobile communications systems?" *IEEE Communications Magazine*, vol. 52, no. 9, pp. 88–95, 2014.

[12] Z. Pi and F. Khan, "An introduction to millimeter-wave mobile broadband systems," *IEEE Communications Magazine*, vol. 49, no. 6, pp. 101–107, 2011.

[13] M. Özen, K. Andersson, and C. Fager, "Symmetrical doherty power amplifier with extended efficiency range," *IEEE Trans. on Microwave Theory and Techniques*, vol. 64, no. 4, pp. 1273–1284, 2016.

[14] J. Wood, *Behavioral Modeling and Linearization of RF Power Amplifiers.* Artech House, 2014.

[15] J. G. Mike Golio, *RF and Microwave Circuits, Measurements, and Modeling.* CRC Press, 2007.

[16] D. H. Wisell, B. Rudlund, and D. Ronnow, "Characterization of memory effects in power amplifiers using digital two-tone measurements," *IEEE Trans. on Instrumentation and Measurement*, vol. 56, no. 6, pp. 2757–2766, 2007.

[17] D. Schreurs, M. O'Droma, A. A. Goacher, and M. Gadringer, *RF Power Amplifier Behavioral Modeling.* Cambridge University Press, 2009.

[18] L. Ding, "Digital predistortion of power amplifiers for wireless applications," Ph.D. dissertation, Georgia Institute of Technology, 3 2004.

[19] S. Haykin and M. Moher, *Communication Systems.* John Wiley and Sons, 2009.

[20] J. C. Pedro and S. A. Maas, "A comparative overview of microwave and wireless power-amplifier behavioral modeling approaches," *IEEE Trans. on Microwave Theory and Techniques*, vol. 53, no. 4, pp. 1150–1163, 2005.

[21] A. Zhu and T. J. Brazil, "An overview of volterra series based behavioral modeling of RF/microwave power amplifiers," in *2006 IEEE Annual Wireless and Microwave Technology Conference*, 2006, pp. 1–5.

[22] F. M. Ghannouchi and O. Hammi, "Behavioral modeling and predistortion," *IEEE Microwave Magazine*, vol. 10, no. 7, pp. 52–64, 2009.

[23] D. R. Morgan, Z. Ma, J. Kim, M. G. Zierdt, and J. Pastalan, "A generalized memory polynomial model for digital predistortion of RF power amplifiers," *IEEE Trans. Signal Process.*, vol. 54, no. 10, pp. 3852–3860, Oct 2006.

[24] L. Ding and G. T. Zhou, "Effects of even-order nonlinear terms on power amplifier modeling and predistortion linearization," *IEEE Trans. on Vehicular Technology*, vol. 53, no. 1, pp. 156–162, 2004.

[25] J. Kim and K. Konstantinou, "Digital predistortion of wideband signals based on power amplifier model with memory," *Electronics Letters*, vol. 37, no. 23, pp. 1417–1418, 2001.

[26] H. Ku and J. S. Kenney, "Behavioral modeling of nonlinear RF power amplifiers considering memory effects," *IEEE Trans. on Microwave Theory and Techniques*, vol. 51, no. 12, pp. 2495–2504, 2003.

[27] H. Cao, A. Soltani Tehrani, C. Fager, T. Eriksson, and H. Zirath, "I/Q imbalance compensation using a nonlinear modeling approach," *IEEE Trans. on Microwave Theory and Techniques*, vol. 57, no. 3, pp. 513–518, 2009.

[28] L. Anttila, P. Handel, and M. Valkama, "Joint mitigation of power amplifier and I/Q modulator impairments in broadband direct-conversion transmitters," *IEEE Trans. Microw. Theory Techn.*, vol. 58, no. 4, pp. 730–739, April 2010.

[29] T. Adali, P. J. Schreier, and L. L. Scharf, "Complex-valued signal processing: The proper way to deal with impropriety," *IEEE Trans. Signal Process.*, vol. 59, no. 11, pp. 5101–5125, 2011.

[30] P. B. Kenington, *High Linearity RF Amplifier Design*, ser. International series of monographs on physics. Artech House, 2000.

[31] J.-H. Tsai, H.-Y. Chang, P.-S. Wu, Y.-L. Lee, T.-W. Huang, and H. Wang, "Design and analysis of a 44-GHz MMIC low-loss built-in linearizer for high-linearity medium power amplifiers," *IEEE Trans. Microw. Theory Techn.*, vol. 54, no. 6, pp. 2487–2496, June 2006.

[32] X. Wu, C. Yu, H. Sun, and X. Zhu, "A millimeter wave digital predistortion platform for linearization of power amplifiers," in *2017 IEEE Asia Pacific Microw. Conf. (APMC)*, Nov 2017, pp. 1066–1068.

[33] R. W. Heath, N. González-Prelcic, S. Rangan, W. Roh, and A. M. Sayeed, "An overview of signal processing techniques for millimeter wave MIMO systems," *IEEE Journal of Selected Topics in Signal Processing*, vol. 10, no. 3, pp. 436–453, 2016.

[34] M. Gavell, G. Granström, C. Fager, S. E. Gunnarsson, M. Ferndahl, and H. Zirath, "An *E*-band analog predistorter and power amplifier MMIC chipset," *IEEE Microw. Wireless Compon. Lett.*, vol. 28, no. 1, pp. 31–33, Jan 2018.

[35] J.-H. Tsai, "A 42-GHz transmitter linearization using predistortion IF amplifier," *Microw. and Opt. Techn. Lett.*, vol. 51, no. 6, pp. 1450–1452, 2009.

[36] A. Katz, M. Chiappetta, and R. Dorval, "Predistortion linearization to 100 GHz," in *2013 IEEE Topical Conf. on RF/Microw. Power Amplifiers for Wireless and Radio App.*, Jan 2013, pp. 34–36.

[37] T. Rahkonen, O. Kursu, M. Riikola, J. Aikio, and T. Tuikkanen, "Performance of an integrated 2.1 GHz analog predistorter," in *2006 International Workshop on Integrated Nonlinear Microwave and Millimetre-Wave Circuits*, Jan 2006, pp. 34–37.

[38] R. N. Braithwaite, "Using a cascade of digital and analog predistortion to linearize a dual-band RF transmitter," *2017 IEEE Topical Conf. on RF/Microw. Power Amplifiers for Wireless and Radio App.*, pp. 77–80, 2017.

[39] J. K. Cavers, "Amplifier linearization using a digital predistorter with fast adaptation and low memory requirements," *IEEE Trans. Veh. Technol.*, vol. 39, no. 4, pp. 374–382, 1990.

[40] P. Jardin and G. Baudoin, "Filter lookup table method for power amplifier linearization," *IEEE Trans. Veh. Technol.*, vol. 56, no. 3, pp. 1076–1087, 2007.

[41] S. N. Ba, K. Waheed, and G. Tong Zhou, "Efficient spacing scheme for a linearly interpolated lookup table predistorter," in *2008 IEEE International Symposium on Circuits and Systems*, 2008, pp. 1512–1515.

[42] C. Crespo-Cadenas, M. J. Madero-Ayora, J. Reina-Tosina, and J. A. Becerra-González, "Transmitter linearization adaptable to power-varying operation," *IEEE Trans. Microw. Theory Techn.*, vol. 65, no. 10, pp. 3624–3632, Oct 2017.

[43] H. Cao, A. Soltani Tehrani, C. Fager, T. Eriksson, and H. Zirath, "Compensation of transmitter distortion using a nonlinear modeling approach," in *2008 International Workshop on Integrated Nonlinear Microwave and Millimetre-Wave Circuits*, Nov 2008, pp. 131–134.

[44] A. Katz, R. Gray, and R. Dorval, "Truly wideband linearization," *IEEE Microw. Mag.*, vol. 10, no. 7, pp. 20–27, Dec 2009.

[45] S.-Y. Lee, Y.-S.Lee, S.-H.Hong, H.-S.Choi, and Y.-H.Jeong, "An adaptive predistortion RF power amplifier with a spectrum monitor for multi-carrier WCDMA applications," *IEEE Trans. on Microwave Theory and Techniques*, vol. 53, no. 2, pp. 786–793, 2005.

[46] J. Potschka, M. Dietz, K. Kolb, T. Maiwald, S. Breun, T. Ackermann, D. Ferling, A. Hagelauer, and R. Weigel, "A highly linear and efficient 28 GHz stacked power amplifier for 5G using analog predistortion in a 130 nm BiCMOS process," in *2019 IEEE Asia-Pacific Microwave Conference (APMC)*, 2019, pp. 920–922.

[47] J. Yi, Y. Yang, M. Park, W. Kang, and B. Kim, "Analog predistortion linearizer for high-power RF amplifiers," *IEEE Trans. on Microwave Theory and Techniques*, vol. 48, no. 12, pp. 2709–2713, 2000.

[48] S.-Y. Lee, Y.-S. Lee, and Y.-H. Jeong, "Fully-automated adaptive analog predistortion power amplifier in WCDMA applications," in *2005 European Microwave Conference*, vol. 2, 2005, pp. 4 pp.–970.

[49] D. Zhou and V. E. DeBrunner, "Novel adaptive nonlinear predistorters based on the direct learning algorithm," *IEEE Trans. on Signal Processing*, vol. 55, no. 1, pp. 120–133, 2007.

[50] M. Schetzen, *The Volterra and Wiener Theories of Nonlinear Systems*. Krieger Publishing Company, 2006.

[51] D. Psaltis, A. Sideris, and A. A. Yamamura, "A multilayered neural network controller," *IEEE Control Systems Magazine*, vol. 8, no. 2, pp. 17–21, 1988.

[52] C. Eun and E. J. Powers, "A new Volterra predistorter based on the indirect learning architecture," *IEEE Trans. on Signal Processing*, vol. 45, no. 1, pp. 223–227, 1997.

[53] J. Harmon and S. G. Wilson, "Iterative approach to the indirect learning architecture for baseband digital predistortion," in *2010 IEEE Global Telecommunications Conference GLOBECOM*, 2010, pp. 1–5.

[54] J. Chani-Cahuana, C. Fager, and T. Eriksson, "A new variant of the indirect learning architecture for the linearization of power amplifiers," in *2015 European Microwave Conference (EuMC)*, 2015, pp. 1295–1298.

Paper A

A Methodology for Analysis of mm-Wave Transmitter Linearization Trade-offs Under Spectrum Constraints

H. V. Hünerli, M. Gavell, P. Taghikhani, and C. Fager

in *Proc. International Workshop on Integrated Nonlinear Nicrowave and mm-wave Circuits*, pp. 1-3, Jun. 2018

Paper B

E-band Transmitter Linearization Using Analog Predistortion

H. V. Hünerli, M. Özen, M. Gavell, and C. Fager

Manuscript